SNAKES AND LABYRINTHS: ADHESION-INDUCED FINGERING INSTABILITIES IN THIN ELASTIC FILMS

SNAKES AND LABYRINTHS: ADHESION-INDUCED FINGERING INSTABILITIES IN THIN ELASTIC FILMS

By

BENJAMIN R. DAVIS-PURCELL, B.Sc.

A Thesis
Submitted to the School of Graduate Studies
in Partial Fulfillment of the Requirements
for the Degree
Master of Science

McMaster University

MASTER OF SCIENCE (2017) McMaster University
(Physics) Hamilton, Ontario

TITLE: Snakes and Labyrinths: Adhesion-induced fingering instabilities in thin elastic films

AUTHOR: Benjamin R. Davis-Purcell, B.Sc. (McMaster University)

SUPERVISOR: Dr. Kari Dalnoki-Veress

NUMBER OF PAGES: ix, 56

Abstract

Fingering instabilities can be observed when studying many different phenomena and display elegant pattern formation. Adhesion-induced fingering instabilities, discovered in the early 2000s, are instability patterns that arise when elastic films are sandwiched between two rigid surfaces. In this thesis we investigate this adhesion-induced fingering instability in thin elastic films. This work builds upon previous research into this instability. Experiments based on studies in the literature were performed to further examine past results; general scaling rules were confirmed, but discrepancies between current and past data show that there is still much to understand theoretically. We also perform novel experiments to elucidate the effects of strain on the instability pattern. It is found that the pattern aligns with the direction of strain in a thin film. We provide a theoretical model to explain this result.

Acknowledgements

When starting a large project, be it a new experiment, initiating a new sports team, or writing a thesis, I tend to leave the most difficult tasks until the end. Completing the simpler tasks of a big project first allows me to get into my groove – then the ideas, emails, and words start flowing. This may explain why my thesis was 'complete' until I realized that this section still simply said "Thanks Mom." It is easy to quickly mentally recognize all the amazing people who helped make this Master's possible, because it is so easy for me to understand that my work over the last two years would never even have started, let alone been completed, if not for these people. It is a much more difficult task to put these thoughts to paper, but I will try.

Without a doubt, I must thank my supervisor Kari. Well before I knew I cared about the field of soft condensed matter, I knew that I wanted Kari as a supervisor. You single-handedly pulled me into this field without open promises or guarantees of success, but simply by being yourself and showing me the beauty of the field and all physics research in general. This happened by way of multiple undergraduate courses, many talks and emails, and a co-op work term, before finally becoming fully sucked into the Master's (perhaps numerous beers and coffees along the way helped). Kari, you have inspired me to become a better physicist, researcher, presenter, science communicator, and person. I will forever thank you for that.

Many other people helped make this document possible. To my friends (and especially roommates over the years), thanks for letting me talk physics when you had no interest in listening (and for when you did too), and sticking around long enough to talk about everything else in life and just hang out. Roommates, thanks for putting up with me when I used the microwave at 5 am after coming home starving from a long day/night of writing. And Fraser, thanks for being my best friend and keeping our careers completely in parallel – hopefully we can continue this trend!

To my lab mates, present and past, thanks for making our research group the best one that I know of (probably just the best one period). A special shout out goes to Mark Ilton for being my first mentor in the group, spending endless hours working with me on projects that were super cool and exciting, but in the end did not come to complete fruition. Additionally, a special thank you goes out to Paul Fowler, who was (and still is) always willing to drop something to assist me with some coding,

Latexing, experiment hype, and most importantly, long walks and talks when I was at my lowest of lows.

Finally, to my family: you were (and are) always there for me and always interested in hearing my specific work, listening patiently as I explained things over and over again, listening to me practise presentations, listening to my crazy philosophical physics arguments, and so on. Mom, Dad, and my two little sisters Rebecca and Leah, thanks for continuing to support me as I know you always will. I love you. Also, I cannot forget my Bubie and Zaida, who always wanted to hear about my physics research and just talk physics (and sci-fi?) in general. I continue to love our discussions in person and over email, and I love you guys too.

Oh, and one more thing: thanks to sports! Hockey, squash, ultimate frisbee, softball, volleyball, and all the rest. Thanks for being my outlet. Now on to the next challenge!

Contents

List of Figures

LIST OF FIGURES

Chapter 1

Introduction

Beautiful patterns naturally occur all around us, spanning all length scales including those that are impossible to view with the naked human eye. One can easily picture the black and white stripes of a zebra or the rippled pattern on the outside of a seashell; these are patterns that are visible with our eyes. There are also larger scale patterns; some examples include the clouds in our atmosphere [1], the bands of gas that form the surface of Jupiter [2], or the exquisite spirals that make up the shape of some galaxies [3]. Of course, small-scale patterns form as well, from the unique pattern of an individual snowflake [4], to the wrinkles that form in a compressed nanoscale membrane [5, 6]. These patterns often form because of competition between two or more forces; if one of the forces becomes the strongest and wins this 'battle', these patterns are often driven to move from the patterned state to a more stable one. Patterns that form in this way are known as instability-driven patterns.

In this thesis, I will discuss my work with one such pattern-forming instability, the adhesion-induced instability in thin elastic films. This instability forms when a soft elastic film is sandwiched between two rigid surfaces. The film is bonded to one of the surfaces, while a gap is established between the other surface and the film. Adhesive contact between the film and non-bonding surface causes the instability to form within the gap [7–15]. In order to properly understand the physics behind this instability, we must first understand the underlying physics of this type of pattern formation, along with the experimental techniques needed to properly create and observe these patterns.

This thesis is structured as follows: Chapter 1 outlines the background physics necessary to understand this adhesion-induced instability. Chapter 2 discusses the key experimental techniques needed to perform thin film instability experiments. Chapter 3 introduces the specific instability that I study, looking at previous work and my first set of experiments examining this instability. Chapter 4 discusses a variation of the instability to examine how this instability forms under strain. Chapter 4 is centred around a manuscript that was written in collaboration with Pierre Soulard, Thomas Salez, and Elie Raphaël, a team of theorists from the ESPCI in France. This work is to be submitted. Chapter 5 will summarize the thesis. This thesis is written so as to provide a detailed starting point to any new student looking to continue studying this instability or a related one.

1.1 Patterning and Instabilities

We see intricate patterns all the time in nature by eye, and that number vastly grows if we use tools that allow us to observe different length scales, such as a telescope for large length scales or a microscope for small ones. At any length scale, when nature presents us with a stunning pattern, we are driven as physicists to try to understand why such a pattern occurs. Beyond this innate yearning for knowledge, why should we study natural patterns? We can learn many things from observing and quantifying these patterns. Often, understanding how a pattern forms increases our knowledge of fundamental physics, teaching us how different interactions occur across various length scales and allowing us to apply this useful knowledge elsewhere [16–18]. In addition to this basic drive to learn, patterning and instabilities can be studied in order to apply what we learn directly to our lives. In this work, we are not concerned with finding an application for our fundamental research, but there certainly are many. In regards to elastic adhesion instabilities such as the one that is the topic of this thesis, direct applications include patterning flexible computer chips [19, 20], increasing traction of car tires [21], improving the performance of running shoes [22, 23], and many more [24].

The adhesion-induced fingering instability is created by confining a thin, soft elastic film between two rigid surfaces; the film is bonded to one of the surfaces,

while the other surface creates a gap between itself and the film. The film is forced to bridge the gap with the non-bonded surface, creating the instability [7–15]. The experiments in this thesis create the instability by indenting elastic films: the elastic film is bonded to a rigid substrate – the lower surface, and the film is indented from above – the upper surface. A fingering instability pattern forms in the upper surface of the film upon indentation. This pattern is then observed with optical microscopy.

Patterning is studied in all areas of science, and often involves non-linear equations [16] that can be cumbersome and sometimes can make the interesting underlying physics difficult to discern. When one studies instability-driven pattern formation, a set of key parameters arise that describe the instability. In our experiments, one such parameter is the wavelength (denoted by λ), which is defined as the spacing between the repeated pattern unit just like the wavelength of a sine wave. Figure 1.1 (a) shows a sample image from one of my experiments, defining the wavelength as the spacing between consecutive fingers. In this figure, the darkest parts of the image are where the film is contacting the upper indenting surface, forming the instability pattern. Figure 1.1 (b) shows a schematic of the indenter that created this instability pattern (more on indenters in section 2.6). I will expand on wavelength measurements more in Ch. 3, where I will also introduce in detail the history of the adhesion-induced instability that is the focus of my work.

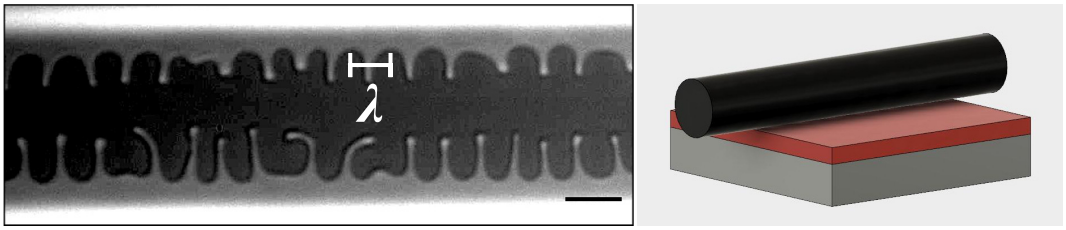

Figure 1.1: (a) A sample fingering instability image showing the definition of a wavelength, λ. The observed pattern is created when a thin elastic film bonded to a rigid substrate is forced to contact an upper indenting surface. (b) Here, the indenting surface is a cylindrical indenter which is shown schematically with a clear glass rod (cylinder) contacting a thin elastic film (red) bonded to a rigid substrate (glass microscope slip). There will be more on indentation in section 2.6. The scale bar in (a) is 10 μm.

1.2 Surface Tension

The driving force behind the pattern formation studied here is adhesion. Adhesion itself will be discussed in more detail in the next section (1.3), but first we need to answer the question: *Why do things preferentially stick to other things?*, or more scientifically, *What causes a fluid/material to flow from one contact to another?* The answer is surface tension.

Materials preferentially adhere to surfaces to minimize their free energy. If a material reduces its free energy when contacting a new surface, it will do so as long as the energy required to deform is not greater than the energy reduction gained from the new contact. This is most easily explained in the case of a liquid. In general, molecular interactions with like particles are favourable. Therefore, a liquid molecule is in an energetically favourable state when it is surrounded by other same-liquid molecules. It is energetically favourable because in a liquid, the self-attraction between liquid molecules is greater than the average thermal vibration of each molecule (the other way around is what we call a gas) [25]. The molecules at the surface of a liquid are in a less energetically favourable state because they lose some contact with their familiar matching molecules in order to interact with the air molecules at the surface.

The same energy-minimizing contact principle can be generalized to any material. Materials rarely preferentially contact air, so surface interactions with air are unfavourable. However, air can be replaced by a more favourable solid or fluid that would reduce the surface energy. If this contact is favourable enough, the base material can adhere to the upper surface and be deformed elastically by retracting this upper material after contact is made. This is the basis of the adhesion-induced fingering instability [7, 8, 24]. In physical terms, surface tension is defined as a force per unit length, or the work required to create interface per unit area:

$$\gamma = \frac{F}{L} = \frac{W}{A}. \tag{1.1}$$

1.3 Adhesion

Dissimilar particles or surfaces have the ability to stick to each other, should it be energetically favourable to do so. We call this adhesion [26–28]. This can be contrasted

with cohesion, the tendency of *similar* particles or surfaces to stick to each other.

When no other forces are present, dissimilar surfaces adhere to each other if this adhering results in an overall free energy reduction. The work of adhesion can be calculated using:

$$W_{ab} = \gamma_a + \gamma_b - \gamma_{ab}, \tag{1.2}$$

where γ_a and γ_b are the surface energies of surfaces a and b, and γ_{ab} is the surface energy of the final combined surface ab. For the contact to be favourable, γ_{ab} must be less than the energy of each individual surface γ_a and γ_b. Surface energy is the work per unit area done by the force that creates the new surface.

Adhesion observed in the instability examined in this thesis is dispersive adhesion. This type of adhesion is when two surfaces are held together due to van der Waals forces. These forces are strongest when two surfaces are very close together. Once separation increases to about 1 nm, the adhesive van der Waals forces quickly begin to decrease. Practically, it is very difficult to bring two surfaces this close to each other. To do so successfully, the surfaces must be uniformly flat and clean, free of any contamination like dust particles. One common household adhesive that successfully adheres to other surfaces is cling wrap, a thin, flat film. Other common adhesives like tape cannot be as thin and smooth as cling wrap so they employ a different adhesion method - chemical adhesion. In chemical adhesion, stronger intermolecular forces like ionic and covalent bonds are formed to hold dissimilar surfaces together.

When studying the adhesion-induced elastic instability, one must model elasticity combined with adhesion. Many models for elasticity plus adhesion incorporate adhesion into contact mechanics models; the most commonly used model that does this effectively is the Johnson-Kendall-Roberts (JKR) model [29]. This model looks at applied forces and adhesion within a single area of contact, similar to pressing down on a surface with a stamp. Since this is the basic setup of all indentation experiments in this thesis (see section 2.6), the JKR theory is one of the starting points for creating the model for finger instability energetics that is discussed in the Theory section of the Ch. 4 paper.

1.4 Stress and Strain

When a force F is applied to a solid along some surface area A, we call this a shear stress σ:

$$\sigma = F/A. \tag{1.3}$$

The solid deforms in response to this stress. We measure this deformation δx parallel to the applied force. The deformation δx is measured relative to the direction normal (y) to the applied force. The ratio of δx to y is known as shear strain, e:

$$e = \frac{\delta x}{y}. \tag{1.4}$$

For a Hookean elastic solid such as the one used in the experiments performed in this thesis, the shear strain is proportional to the shear stress with the proportionality factor being the shear modulus μ. (We note that the elastic solid used in the experiments in this thesis is not exactly Hookean, but can be approximated as a Hookean solid). The shear modulus is a material property that controls its deformability. We can therefore define shear strain as

$$e = \frac{\sigma}{\mu}. \tag{1.5}$$

When calculating stress and strain in elastic materials, we must go beyond this simplistic model. In general, a force will not be applied to a surface along one principal axis. In fact, there can be two perpendicular components of applied force to every principal axis (just as in a three-coordinate system, both y and z are perpendicular to x). This leads to a more accurate definition of stress in the form of a symmetric *stress tensor*. Additionally, when a material is deformed, each position in the material is changed relative to some initial reference position. For this reason, the change in length between any two points must be defined. In three dimensions, this amounts to a 3×3 diagonalizable matrix known as the *strain tensor*. The theory in the paper presented in Chapter 4 uses these more detailed definitions to accurately calculate stress and strain. One can conduct an in-depth study on the mathematics of stress and strain by following *Landau & Lifshitz* [30] and *Timoshenko & Goodier* [31].

1.5 Elastocapillarity

When two competing interactions are simultaneously acting in a system, their relative strengths can be compared to determine the scale at which each interaction is most important. For example, a drop of water dangling on the edge of a faucet will only fall if it has enough mass for gravity to overcome the water's attraction to the faucet. Similarly, surface tension (and the reduction in energy obtained by contacting a favourable material) will only cause a material to deform if the strength of surface tension is greater than a material's resistance to the deformation i.e. its shear modulus. Elastocapillarity is the study of these two interactions.

Surface tension γ and shear modulus μ can be compared to extract a length scale at which both surface attraction and resistance to deformation become important. This length scale is called the elastocapillary length and is defined by γ/μ. When working at length scales significantly greater than a material's elastocapillary length, only surface interactions are important and the resistance to deformation can generally be neglected. Similarly, at length scales significantly less than a material's elastocapillary length, only the deformation energy is important and a material will struggle to deform at all due to surface forces. However, when working at length scales comparable to a material's elastocapillary length, both interactions are important, and interesting effects occur [32–35].

Elastocapillarity is currently a heavily studied area of research in soft matter physics. Some recent highlights are noted in Ch. 4. In regards to the study of the adhesion-induced fingering instability, the ratio between elastocapillary length and film thickness becomes important when looking at specific wavelength scaling regimes. This will be discussed in Ch. 3.

1.6 Polymers

Polymers are long chain molecules made of repeated subunits called monomers that are covalently bonded together. Many of the materials that we interact with in daily life are made of polymers: this includes abiotic materials like plastics and rubbers, along with biotic materials like DNA strands. There are many different types of polymers, but my thesis work focused on observing the adhesion-induced fingering

instability using one type of polymer called styrene-isoprene-styrene (SIS).

SIS belongs to a special class of polymers known as block copolymers. Block copolymers are polymers composed of two or more sets of repeated monomers. For example, polystyrene is a polymer made of repeated styrene subunits. Let us call this polymer A. Polyisoprene is a polymer composed of repeated isoprene subunits; we will call this polymer B. An example of a diblock copolymer would be a chain of styrene molecules connected to a chain of isoprene molecules – an AB block. SIS is a triblock copolymer, meaning there are three polymer chains of two types of polymers, ABA. A sketch of this is shown in fig. 1.2. Block polymers like SIS tend to self-organize

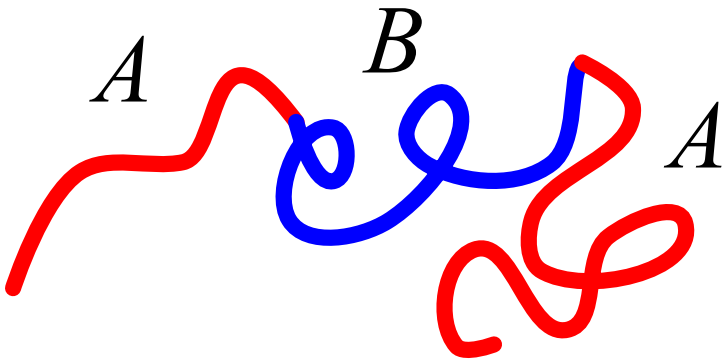

Figure 1.2: Sketch of a triblock copolymer such as SIS.

into specific configurations based on the interactions between the A components and the B components [36].

One special property of polymers is that they have a glass transition temperature, T_g. Above this temperature, the polymer is free to flow over time, meaning the polymer acts like a fluid with the flow rate determined by its viscosity. Below the glass transition temperature, the polymer is said to be in its 'glassy' state, meaning it does not flow over accessible timescales and acts like a solid. One can manipulate a polymer so that it is in a non-equilibrium state (not the free energy minimizing state), and the polymer will remain in that state if it is 'frozen' below its glass transition temperature. If the polymer is heated above its glass transition temperature, it will flow to reach an equilibrium state, minimizing its free energy. In block copolymers, each individual polymer composing the block has its own glass transition temperature. The glass transition temperature of polystyrene is about 100°C, while the glass transition

temperature of polyisoprene is about $-65°C$. This T_g difference, along with the 14% styrene to isoprene composition ratio of the SIS used in all experiments of this thesis, causes room temperature SIS to have a glassy styrene component and a liquid-like isoprene component. The SIS triblock self-organizes to form spherical glassy styrene components that are loosely held together by long crosslinked liquid-like isoprene chains.

1.6.1 Elastomers

SIS is classified as a special type of polymer (at room temperature) known as an elastomer due to its composition discussed in the previous section. Elastomers are polymers that have very weak inter-molecular forces, low shear moduli, and high failure strain, giving them elastic properties. One common example of this is rubber. These elastic properties come from the fact that elastomers contain polymers in the glassy state as well as the liquid state, allowing the molecules to remain bound together while having stretchy, malleable properties. Elastomers are soft and deformable, and therefore make excellent adhesives and sealants because they can sustain high levels of strain without breaking.

1.6.2 Thin Films

Polymers that are confined to thin films (film thickness $h \sim \text{nms} - \mu\text{ms}$) exhibit different properties compared to polymers in the bulk [37–40]. Two important differences are as follows: firstly, in thin films, polymer chains have less space to move around as they are confined to a more restricted volume; secondly, surface forces become more important in thin films because the surface to volume ratio is much greater in thin films versus polymers in the bulk. All polymers used in this thesis are confined to thin films – another reason why surface tension is so important as a driving force for this instability as will be explained in detail later in this thesis. Spincoating, the method used to prepare thin films, is discussed in Ch. 2 section 2.1.

Chapter 2

Experimental Details

This section describes the experimental techniques required to perform the experiments in Chapters 3 and 4. Chapter 4 explains many aspects of the strained indentation experiments, so when specifically describing these experiments I will only discuss the important details that were excluded from the manuscript. Since experimental length scales are often on the order of the size of dust particles, cleanliness is important. Whenever possible, samples were prepared under a laminar flow hood. Experiments were performed promptly after sample preparation, and latex gloves were always worn.

2.1 Spincoating

All experiments in this thesis begin with a thin film on a substrate. Spincoating is the optimal way to make a uniform thin film, and is the method used for all thin film preparation in this thesis.

Spincoating is the process that takes a polymer-solvent solution and turns it into a thin film. The first step in this process is to make the polymer solution. In general, one can make any polymer solution by mixing the desired polymer with a solvent for that specific polymer. The ratio of polymer to solvent is the main factor affecting the eventual thickness of the film that will be made. All experiments in this thesis use exclusively styrene-isoprene-styrene (SIS) triblock copolymer (14% styrene content, Sigma Aldrich) dissolved in toluene (Fisher Scientific, Optima grade). Toluene is

filtered with 0.2 mm Milipore filters (Millex) and then added to SIS in a small sample beaker. This mixture is then placed on a shaker for at least 24 hours so that the polymer becomes completely solvated to make a uniform solution. Solutions ranged from 1% SIS in toluene to 15% SIS in toluene.

Once solutions are sufficiently dissolved, they are filtered again with the Milipore filters. Solutions with a SIS in toluene ratio of 7% or greater were left unfiltered, as filtering at these high percentages is not possible due to the liquid's high viscosity. Once the final solution is prepared, spincoating can begin. A substrate (see section 2.2) is placed on a chuck and then a drop of the solution is pipetted onto the substrate so that the substrate's surface area is completely covered by solution. The chuck then accelerates to rotate at high speeds of 2000 rpm to 6000 rpm for 20 seconds. This initial acceleration ejects excess solvent. Then, as the chuck rotates, solvent evaporates from the solution leaving a thin uniform film on the substrate. The rotation speed of the chuck also affects the final film thickness (faster rotation speed produces a thinner film). Using the stated range of solution concentrations and rotation speeds, spincoated SIS films ranged in thickness from about 40 nm to 4000 nm. Figure 2.1 shows a schematic of the spincoating process.

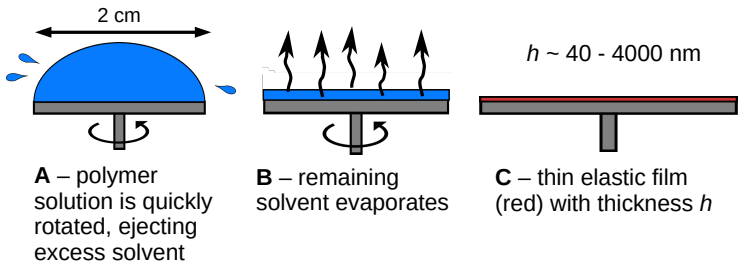

Figure 2.1: Schematic of the spincoating process.

2.2 Substrates

Substrates are the lower surface onto which solutions are spincoated to become thin films. Three different substrates were used for the purposes of thin film experiments in this thesis. Silicon (Si) wafers are the optimal substrate to measure thicknesses of films using ellipsometry (section 2.5), and that is the sole purpose of Si substrates for

experiments performed in this thesis. Each time a thin film sample was prepared for experimentation, an additional film was prepared on Si to measure thickness. Silicon substrates used for this purpose were approximately 1 cm $\times$ 1 cm.

Another common utility substrate is mica, which is a layered silicate sheet material that can be cleaved with a scalpel such that the resulting mica sheet is atomically flat at its surface. Mica is useful because spincoated films can be floated (further details on floating can be found in section 2.4) off of its surface onto a water bath, making mica useful for transferring films. All stretching experiments (Chapter 4) began with films spincoated onto mica. All mica substrates that were used were approximately 2.5 cm $\times$ 2.5 cm.

The third substrate used for experiments was glass – ordinary clear glass microscope cover slips. Solutions can be spincoated directly onto glass, which allows for *in situ* viewing of a film. All thin films used in Chapter 3 were spincoated onto glass substrates so that they could be observed *in situ* from below using an inverted optical microscope during the indentation process (see section 2.6). These glass microscope cover slips were 2.2 cm $\times$ 2.2 cm. Additionally, all films used in Chapter 4 were transferred to glass substrates after the straining process, before indentation. These glass substrates were 5 cm $\times$ 2.4 cm.

2.3 Annealing

During the spincoating process, polymer molecules incur internal stresses resulting in non-equilibrium chain conformations in the thin film. It is important for the polymer chains to be in their relaxed thin film state before any further experimentation is performed in order to ensure that experimental results are not affected by pre-stresses incurred during the spincoating process. This is especially important for my thesis work, as any pre-strain in the thin films affects the resulting instability pattern that forms upon indentation. Therefore, films must be treated so as to relax their polymer chains after spincoating before the next step in any experiment can be performed. In addition, excess solvent remains in films after spincoating which affects the material properties of the film such as surface tension.

To relax polymer chains and remove excess solvent, all thin films used in this thesis

were annealed at 108°C for 15 minutes. This temperature was chosen because it is above the glass transition temperature of both components of the SIS triblock, but it is not too hot so as to degrade the polymer. It was found that these temperature and time parameters were the optimal ones to ensure that polymer chains were in their relaxed state with minimal excess solvent in the films, while maintaining the films' structural integrity.

2.4 Floating

Floating is the process of transferring a spincoated film from a substrate onto a water bath. These free-standing films can then be picked up by different substrates, floated back onto the original substrate, stacked on top of other films, along with many other innovative experimental techniques. In this thesis, a specific floating process is used for experiments in Chapter 4 in order to allow films to be transferred from a mica sheet to the stretching setup.

All experiments in Chapter 4 require a thin film to be transferred from a substrate onto the custom-built stretching setup (see section 2.7 for more on straining films). To do this, a specific floating process was employed. This process begins with an SIS film that has been spincoated onto mica. Three edges of the film were wiped away using a cotton-tipped applicator soaked in acetone (a few millimetres of film from each edge was wiped away). The fourth edge was then lightly scored with a scalpel, again a few millimetres in from the edge. The mica sheet was then picked up with self-closing tweezers on the scalpel-cut edge and slowly lowered into an ultra-pure water bath (18.2 $M\Omega \cdot cm$) at a 45 degree angle. As the mica crosses the water surface, the SIS film begins to detach from the mica sheet and remains floating on the surface of the water bath. The mica was continually lowered deeper into the water bath at this angle until the SIS film was only attached to the mica sheet at the scalpel-scored edge. At this point, the mica was then slowly retracted from the water at the same 45 degree angle until the original SIS film was back on the mica sheet. This 'self-floating' process traps a thin layer of water that separates the SIS film from the mica surface and allows for easy transfer to the stretching setup. Final transfer to the stretching setup is performed by flipping the mica (still held by tweezers) over

and placing it in the centre of the stretching material (see section 2.7). The floating process is shown schematically in fig. 2.2.

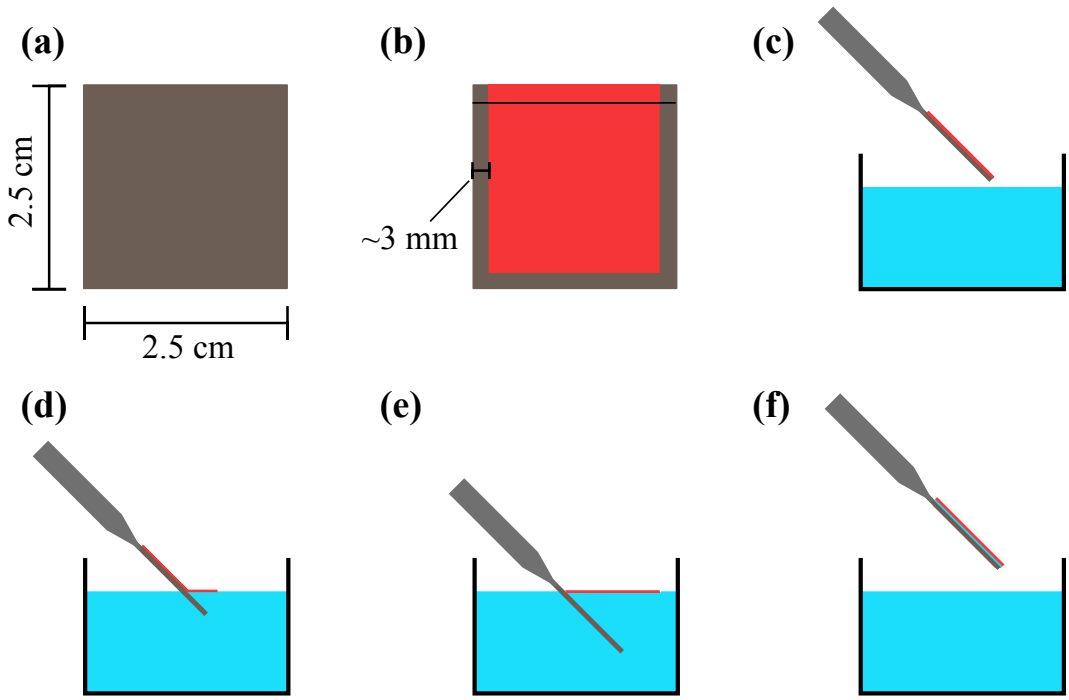

Figure 2.2: Schematic of the floating process. (a) – the mica substrate is shown (brown). (b) – the SIS film (red) has been spincoated onto the mica substrate. Three edges of the SIS film have been wiped away with acetone, while the fourth edge has been scored with a scalpel. (c) – the mica-film bilayer is picked up with tweezers. The water bath is also shown. (d) – the mica is lowered below the surface of the water bath. The SIS film remains on the surface of the water. (e) – the mica is completely submerged in water while the SIS film remains on the water surface. The SIS is still attached to the mica on one edge. (f) – the mica is removed from the water bath. We are left with a mica-water-SIS trilayer.

2.5 Ellipsometry

Ellipsometry is a common optical technique used to measure thin film properties. For the purpose of this thesis, an ellipsometer was only used to measure the thicknesses of thin films on silicon wafers.

The ellipsometer (Accurion, EP3) used for all film thickness measurements in this

thesis is quite simple to use. One must simply turn the machine on, place a thin film (spincoated on silicon) sample under the laser, focus the laser, and press go. Pre-calibrated analysis software is then used to determine the thickness of the film along with its refractive index. Behind the scenes, the operation is much more complex.

An ellipsometer works by bouncing a monochromatic light source off of a sample and detecting the reflected light. The best light source is a laser, since collimated light with minimal beam divergence is desired. This laser light first passes through a polarizer, linearly polarizing the previously unpolarized or randomly polarized light. Next, the light passes through a quarter-wave plate called a compensator that elliptically polarizes the light. The elliptically polarized light is then reflected off the sample at an angle. Upon interaction with the sample, the elliptically polarized light becomes linearly polarized given a specific incident ellipticity determined by the sample's material properties. The reflected linearly polarized light passes through an analyzer (a word for a second polarizer) for cross-polarization, where the analyzer is rotated until a null intensity is measured by the detector. This basic ellipsometry setup, known as a nulling ellipsometer, is shown schematically in fig. 2.3. The reflected light off of

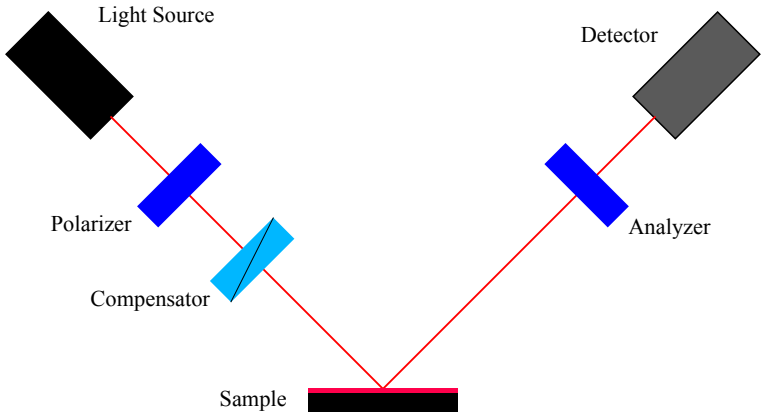

Figure 2.3: Schematic of a basic ellipsometer.

the sample is only linearly polarized for a specific ellipticity of polarized light incident onto the sample. To make a measurement, the polarizer and analyzer are both rotated until the null is detected, which can only occur when the sample-dependent elliptically polarized incident light converts to linear polarized light upon reflection. The conditions for null intensity depend on the angle of incidence of the elliptically

polarized light onto the sample and the reflection properties of the sample that is to be measured. Once the polarizer and analyzer angles are known, along with the angle of incidence, one is able to infer surface properties of the sample.

Film thickness is measured indirectly by way of a model. An ellipsometer directly measures the intensity of light and the angles of the polarizer and analyzer at which a null intensity occurs; film thickness has some dependence on these optical properties. A model is pre-loaded into analysis software given some known quantities such as the wavelength of the laser light and the angle of incidence. These quantities along with the experimentally measured parameters are then input into the model for film thickness to find the best fit to the data. It is through this best fit that the film thickness is finally obtained [41–43]. Using this method, it takes approximately 15 minutes to obtain the thickness of a single film.

2.6 Indentation

Indentation is important for all experiments performed in this thesis because this contact initiation is what causes the adhesion-induced fingering instability to appear. For the purposes of this thesis, indentation is defined as *contacting a film from above with an indenter*. When contact is made, a circular or linear contact patch becomes visible. The fingering instability forms some distance away from the initial contact patch since a gap between the film and indenter is necessary for instability formation (more on this in Chapter 3). Once a thin SIS film has been prepared following the previous steps in this section, the film is placed on an inverted optical microscope and then indented so that the instability pattern forms (films prepared for Chapter 4 were strained (section 2.7) before indentation). The pattern is viewed from below through the microscope.

Two different indenter geometries were used: cylindrical indenters and spherical indenters (shown schematically in fig. 2.4). Cylindrical indenters produce linear contact patches and fingering instability patterns that grow perpendicularly outwards from the centre contact line, while spherical indenters produce circular contact patches and fingering instability patterns that grow radially outward from these centre circular contact patches. The experiments described in Chapter 3 use cylindrical indentation,

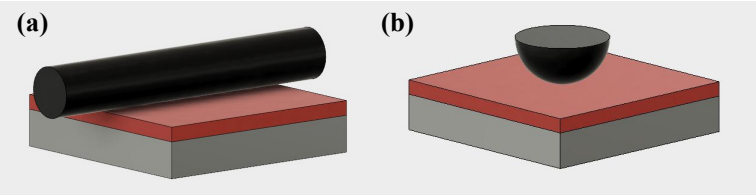

Figure 2.4: Schematic of the two types of indenters contacting a thin film sample. (a) shows the glass rod which acts as a cylindrical indenter. (b) shows the spherical glass lens which acts as a spherical indenter.

while the experiments described in Chapter 4 use spherical indentation.

Two different cylindrical indentation methods were used for the experiments in Chapter 3. In the first method, a long, thin glass rod was placed on top of the SIS film to act as the cylindrical indenter. Gravity provided a strong enough indentation force for the instability to develop. In the second method, a plano-convex cylindrical lens (ThorLabs Inc., 22 mm by 20 mm and focal length of 250 mm) was placed on top of the film to act as the indenter (convex side down to contact the film). A precision actuator (Burleigh 8200 Inchworm) then lowered a flat screw head onto the flat side of the lens, indenting the convex side of the lens into the film. The resulting instability pattern was then observed. This indentation setup is shown schematically in fig. 2.5 (a).

The experiments in Chapter 4 employ spherical indentation. In this set of experiments, a plano-convex spherical lens (ThorLabs Inc., with a diameter of 6 mm and focal length of 30 mm) was used as the indenter. Here, the flat part of the lens was glued to the flat head of a screw. This allowed for precision spherical indentation using the precision actuator, as the lens attached to the screw was lowered as one piece, indenting the film to create a radial fingering instability pattern. This indentation setup is shown schematically in fig. 2.5 (b)

Upon indentation and the formation of the instability pattern, images were recorded with a camera (AVT GigE Vision GT1660) that was attached to the optical microscope. After each sample indentation (for each indentation method), the indenter was retracted and placed on a new, unperturbed film location. Each film was indented three to seven times with multiple images taken per indentation. These images are the raw experimental data that then must be analyzed. Analysis methods are discussed

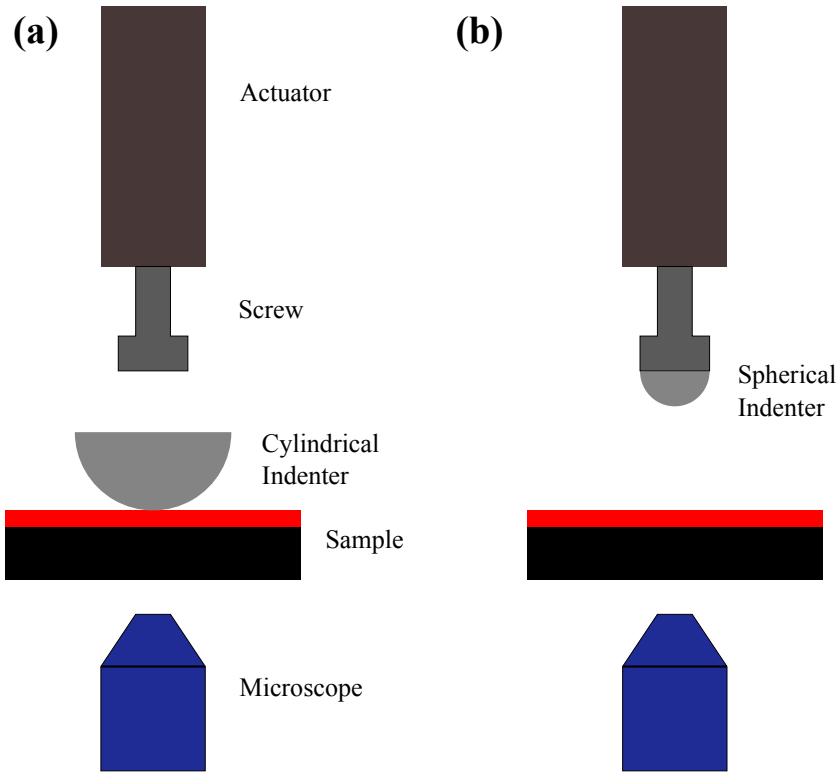

Figure 2.5: Schematic of the general indentation setup used to indent films and observe the instability pattern. (a) shows the second method where the cylindrical indenter sits on the film and is pressed into the film by the screw. (b) shows the third method where the spherical indenter is attached to the screw before indentation.

in Chapters 3 and 4.

2.7 Straining Films

Chapter 4 examines the fingering instability in SIS films under strain. In order to do this, the films must be strained in a reliable, systematic way. This is discussed in detail in Ch. 4, so it will only be briefly touched on here.

After the floating process (section 2.4), films were transferred to a custom-built straining setup. The straining setup is made of a sheet of Elastosil (Wacker Chemie, $h = 200\ \mu$m), a large uniform thickness elastic film that is compliant but remains tense when stretched. This film is cut to a specific shape (see figs. 2.6 & 2.7) so that a uniform stress is applied – this shape includes a central hole where the SIS film is

placed. The Elastosil is clamped down by its four edges to adjustable arms, allowing the film to be stretched along two axes. The strain setup is shown schematically in fig. 2.6 and an actual photograph of the setup is included in fig. 2.7.

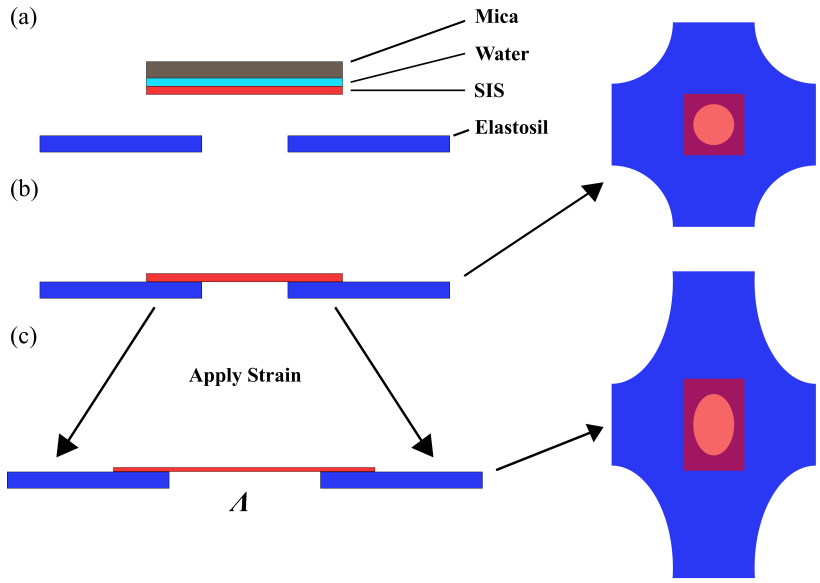

Figure 2.6: Schematic of the custom-built stretching setup. (a) After the floating process, a thin layer of water remains between the mica sheet and the SIS film to allow for smooth transfer to the Elastosil sheet. (b) The SIS film is unstrained on the Elastosil; a corresponding top view is shown. (c) A uniaxial strain is applied, causing the hole to transition from a circle to an ellipse, uniformly straining the SIS film by a factor Λ.

SIS films were transferred by placing the SIS-water-mica trilayer onto the central hole in the Elastosil so that the square film completely covered the circular hole. The mica was then smoothly peeled off, as the addition of the water layer makes it energetically favourable for the SIS to contact the Elastosil over the water-covered mica. After this transfer process, a free-standing SIS film remains. These free-standing SIS films were then uniaxially strained by extending the arms holding the clamped Elastosil along one axis while holding the perpendicular arms to a constant length. This causes the circular central hole to become increasingly elliptical with increasing

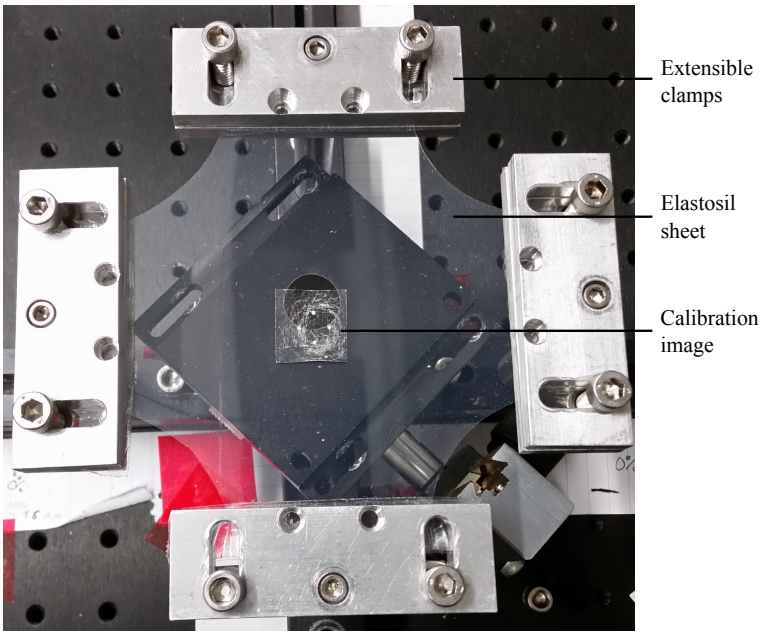

Figure 2.7: Photograph of the custom-built stretching setup. Extensible clamps hold the Elastosil sheet in place allowing for controlled uniaxial strains. The thin film sample is placed over the central hole. Photographs of the calibration pattern underneath the hole are taken before and after the film is strained in order to measure the strain in the film with a custom Matlab code.

strain. We measure strain using the extension parameter Λ, where the length L of the strained material along the strained axis is given by $L_{final} = \Lambda L_{initial}$. Strains were imparted into films such that Λ ranged from 1 to 1.6. SIS films experience material failure at strains greater than $\Lambda \approx 1.6$. Once a film was strained, a glass microscope slide was brought into contact with the film from above. SIS preferentially contacts glass over Elastosil, so carefully laying the glass slide on top of the strained SIS film such that it was completely covered caused perfect contact to be made between the SIS film and the glass. The glass slide was then lifted off of the Elastosil and brought to the microscope for indentation. Pictures were taken of the central hole and calibration pattern before and after straining and then analyzed with a custom Matlab code. The code uses the hole shape and calibration pattern to measure the ellipticity in the hole post-strain relative to pre-strain. The major and minor axis of the hole are measured relative to corresponding axes on the calibration pattern before straining, and the same is done after straining. The ratio of post-strain length difference to

pre-strain length difference along the strained axis gives the ellipticity.

Chapter 3

Adhesion-Induced Fingering Instabilities

In this chapter I discuss the adhesion-induced fingering instability. After outlining some fundamental physics involved in understanding this instability in Chapter 1, and discussing all experimental techniques used to study this instability in Chapter 2, I will now present in detail the instability itself. The introduction summarizes previous work on this instability and gives motivation for its study. The following section discusses my work on this instability that attempts to corroborate previous results. I outline two different sets of experiments that examine the most well-studied parameter of this instability: wavelength (λ) and its dependence on film thickness (h) and present the findings. I find that I can reproduce the general wavelength dependence on film thickness that is in agreement with the literature, but there is some discrepancy between my data and previous literature work. I suggest experiments to further probe this issue in the conclusion, noting that the focus of this thesis is the study of the adhesion-induced instability under strain (anisotropic instability growth), so control parameters were not optimized to examine the previously well-studied dependence of this instability's wavelength as a function of film thickness. However, it is still important to understand the isotropic instability in order to characterize the system.

3.1 Introduction

In the early 2000s, two groups independently discovered beautiful pattern formation in thin, soft elastic films while studying elastic instabilities. The results came out of Lehigh University [7] and the University of Ulm [8]. This pattern formation became known as the adhesion-induced instability in thin elastic films.

The adhesion-induced fingering instability forms when a thin, soft elastic film is sandwiched between two rigid surfaces. Experimentally, this is done by bonding an elastomeric film to a lower rigid substrate and then bringing an upper glass indenting surface into contact with the elastomeric film. When contact is made, the elastomer preferentially contacts the indenting glass surface over air. Some distance away from this initial contact area, a gap exists between the film and the indenter. This gap is where the instability forms, as the film is pulled up to contact the upper indenting surface, but cannot deform more than its elastic modulus will allow. Volume must be conserved, so a depletion region follows next to the initial contact, which is then followed by another contact patch. This pattern repeats itself until the gap between the film and the upper indenter becomes too great and it is no longer energetically favourable for the film to deform to spread the gap. When viewed from above or below, this instability pattern appears as intricate labyrinths, fingers and/or more complex morphologies that have a natural spacing which is the wavelength (λ) of the instability.

The elastomeric film is most commonly made by crosslinking a polymer between two glass slides of differing surface energies (the technique used in [7]) or by spincoating onto a lower substrate (the technique used in [8], as well as all of the experiments performed in this thesis). The crosslinking method is most effective when making thicker films ($h > 4\mu$m) while spincoating is more effective when making thin films ($h < 4\mu$m). Once the thin film sample has been prepared, an upper surface is then brought into contact with the film. This upper surface is commonly a glass microscope slide. The key to instability formation is establishing a gap, which can be manually created by way of a spacer [7] or by inducing some curvature in the indenter [8]. The instability pattern forms in this gap and is then observed with optical microscopy. Both groups involved in the discovery of this instability examined its wavelength as a function of film thickness, and found that λ scales linearly with h [7, 8].

Since its discovery, many studies have examined various aspects of this instability while continuing to measure the wavelength dependence. These studies include but are not limited to: observing spiral labyrinth instabilities by rotating the upper indenting surface [9]; controlling for the flexibility of the upper indenter as well as for the applied force pushing the indenter into the film [9]; observing the instability in an elastic bilayer [44]; examining instability morphology under an electric field [45]; forming the instability on a patterned substrate [46]. Many research groups have also performed simulations to go along with experiments [10, 14, 47, 48]. A recent review paper by Chaudhury *et al.* [24] summarized many of these results and others, while also commenting on future useful studies to better understand various important aspects of the instability. One such aspect that had only been qualitatively studied [11] but lacked a thorough quantitative analysis was the investigation of instability formation in films under strain – this is the focus of this thesis and is addressed in detail in Chapter 4.

All of these previous studies found that λ scales linearly with h. As has been mentioned, the key to instability formation is establishing a gap between the thin elastic film and the upper indenter. This can be done by way of a spacer, by peeling off a contacting surface, by indenting the film and then retracting the indenter, as well as other methods. Varying the gap creating method leads to varying instability morphologies, from fingers and labyrinths to circular blisters. Chaudhury *et al.* [24] compiled these results from different studies to show that wavelength scales linearly with film thickness independent of gap formation method, and found the best fit to all experimental data to be $\lambda = 3.8h$.

This instability develops because the adhesive contact between the elastomer and the indenting surface reduces the system's free energy, but this reduction is counteracted by an increase in free energy due to elastic deformation. The interaction between this adhesive contact energetic gain and elastic deformation energetic cost along with volume conservation causes the instability to develop. The relationship between wavelength and film thickness has been extensively studied theoretically through formal analyses of the dominant wavelength of instability [7, 8, 11, 14, 15, 24, 48–51], which I will not discuss here as the detailed theoretical work is outside the scope of this thesis. All studies were able to confirm the experimental scaling results, showing that

$\lambda = nh$, with $n \geq 2.96$. However due to its complexity, no theory has been able to provide an exact solution for wavelength as a function of film thickness, making the experimental best fit the most reliable comparison tool. Vilmin *et al.* [12] provided a more simple scaling model using fracture mechanics and scaling laws, comparing the energy gained by forming an instability bubble with the energy cost associated with elastic deformation, all under the confines of volume conservation. They were able to obtain a scaling result that was similar to previous work, finding $\lambda \approx 4h$, while providing a more intuitive understanding of the physics. This was done by using the fact that the thin film is incompressible, and by noting that the maximum size of the stress-relaxing instability bubble is limited by and therefore proportional to the thickness of the film. One issue with the theory was made prominent by Gonuguntla *et al.* [10], who studied the instability by working with thinner films than in previous studies. Most experiments used elastic films with $h \sim \mu\text{m} - \text{mm}$, whereas Gonuguntla *et al.* focused on films with $h < 1$ μm. They determined that for this film thickness regime, the elastocapillary length γ/μ of the thin film material becomes important and causes λ to diverge from its linear scaling, becoming nonlinear with h and including a dependence on γ/μ. Chakrabarti and Chaudhury [13] followed up on the work in [10]. They showed that films must be soft (low μ) in order to follow a nonlinear scaling law, and outlined three distinct wavelength scaling regimes based on the ratio of γ/μ to h. These three regimes are as follows:

$$\frac{\gamma}{\mu} \ll h\text{: } \lambda \sim h \tag{3.1a}$$

$$\frac{\gamma}{\mu} \lesssim h\text{: } \lambda \sim h + \gamma/4\mu \tag{3.1b}$$

$$\frac{\gamma}{\mu} \gg h\text{: } \lambda \sim \left(\gamma h^3/\mu\right)^{1/4}. \tag{3.1c}$$

Experiments in [13] found that $\lambda \approx 7h$ due to elastocapillary effects. This result showed that while reproducible experimentally and theoretically, a complete understanding of the instability remains elusive, especially for thin ($h \lesssim \mu$m) films.

Since there are many ways to study this adhesion-induced instability, the work in this thesis was initiated by experiments that attempted to replicate previous results in the literature before novel experiments were conducted. This is what is discussed in

the following section – experiments I performed that were inspired by previous work that attempt to corroborate previous wavelength scaling results, but with a focus on thin films ($h < 4$ μm) for which the wavelength scaling is not clearly understood. Chapter 4 then directly addresses one of the outstanding questions in the literature in regards to this instability: *how does the instability pattern change as a function of film pre-strain?*.

3.2 Indentation Experiments

I performed two different sets of indentation experiments; the goal of each set of experiments was to measure the wavelength of the adhesion-induced fingering instability in thin SIS films as a function of film thickness. This was done to ensure that the results were robust, as changing the way in which the instability forms, or using different analysis techniques should not change the wavelength measurement, as has been previously shown [24]. Experimental details are outlined in Chapter 2, so the reader will be guided to that chapter for clarification of experimental setup. This section briefly outlines the individual experiments and their data collection methods (3.2.1) and then combines the results onto one master plot of wavelength versus film thickness to discuss (3.2.2).

3.2.1 Data Acquisition

In the first set of indentation experiments, SIS films spincoated on glass microscope slides were indented with a thin glass rod to act as a cylindrical indenter (see section 2.6 for more information). This indentation method creates a fingering instability pattern that grows perpendicularly outward from the centre contact line. 19 different SIS films were indented, with film thicknesses ranging from 38 nm to 3850 nm. It is well known (section 3.1) that wavelength increases as a function of film thickness. This can be seen in the sample images shown in fig. 3.1. One can also observe the centre contact line from the length of the cylindrical indenter, along with the fact that the fingers have distinct maximum amplitudes due to the curvature of the cylindrical rod: as the indenter curves away from the film, the gap spacing becomes too large and the instability pattern cuts off. The curvature of the cylindrical indenter can also

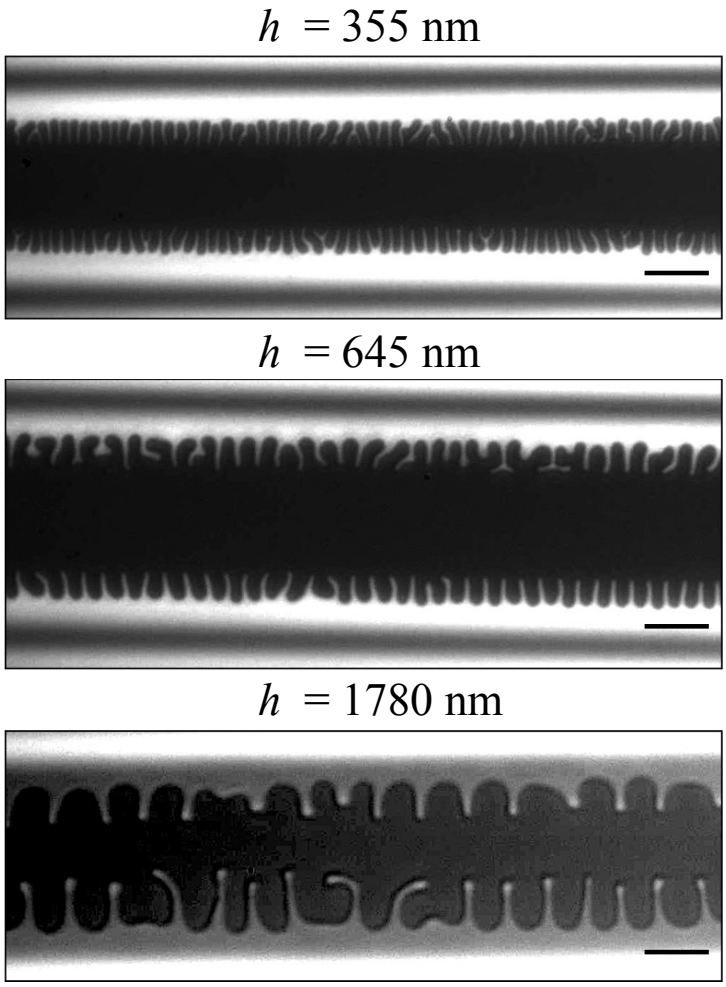

Figure 3.1: Sample images of the instability pattern formed via cylindrical indentation with a thin glass rod. The images have been contrast-edited so the patterns are easier to see. Scale bars are 10 μm.

be indirectly seen by viewing the light and dark fringes in the fig. 3.1 images. This is an optical interference effect coming from the microscope light passing through the curved glass cylinder.

Wavelength measurements were made by directly measuring the distance between five to thirty fingers using a MATLAB image analysis tool. This measurement was made multiple times for each image, and multiple images were taken per film. All of the measured wavelengths for a given film thickness were then averaged, with the error given by the standard deviation. This set of experiments was the most robust

in terms of measuring wavelength, as the greatest number of films were measured (compared to the other two sets of experiments), and the measurements covered the maximum range of the parameter space. Films with $h \lesssim 40$ nm create instability patterns that are very difficult to resolve optically. Uniform films with $h > 4$ μm cannot be easily made by way of spincoating.

The second set of indentation experiments also began by spincoating SIS onto glass microscope slides. Once the thin films were prepared, each film was indented with a cylindrical lens acting as a cylindrical indenter. The cylindrical indenter for these experiments had a much larger radius of curvature than that of the cylindrical rod acting as the cylindrical indenter in the first set of experiments. Due to this setup, the instability pattern that formed in these experiments was an intricate labyrinth pattern. This was because when using this indenter, the gap spacing from the centre contact line increases at a much slower rate (as a function of perpendicular distance from the central contact line) compared to the much thinner cylindrical indentation rod. Thirteen films were indented, with film thicknesses ranging from 120 nm to 2670 nm. Sample images of the observed patterns can be seen in fig. 3.2 (a).

It is more difficult to measure wavelength by hand when the pattern is mostly labyrinth-like (as seen in fig. 3.2 (a)) as opposed to consistent rows of fingers (as seen in fig. 3.1). Instead of using the measurement method discussed above, wavelength in this set of lens indentation experiments was measured by taking the two-dimensional fast Fourier transform (FFT) of each image. The FFT takes the image to inverse length space, creating a Fourier ring. The radial distance from the centre of the FFT image to the centre of the Fourier ring is the inverse wavelength – the FFT turns the dominant repeated pattern in the original image into a ring that encodes the spacing of this pattern. A custom MATLAB code was written for this analysis. First, the raw image was cropped to a square, and the pixel intensities were scaled from 0 to 1 to remove any variation effects from the microscope light between images. The scaled image was then *windowed*. Windowing is a common Fourier transform technique performed prior to taking the FFT that reduces the background intensity in the resulting FFT by darkening the edges of the image to be analyzed. The FFT of the windowed image was taken. Next, the FFT pixels were divided into 1000 bins

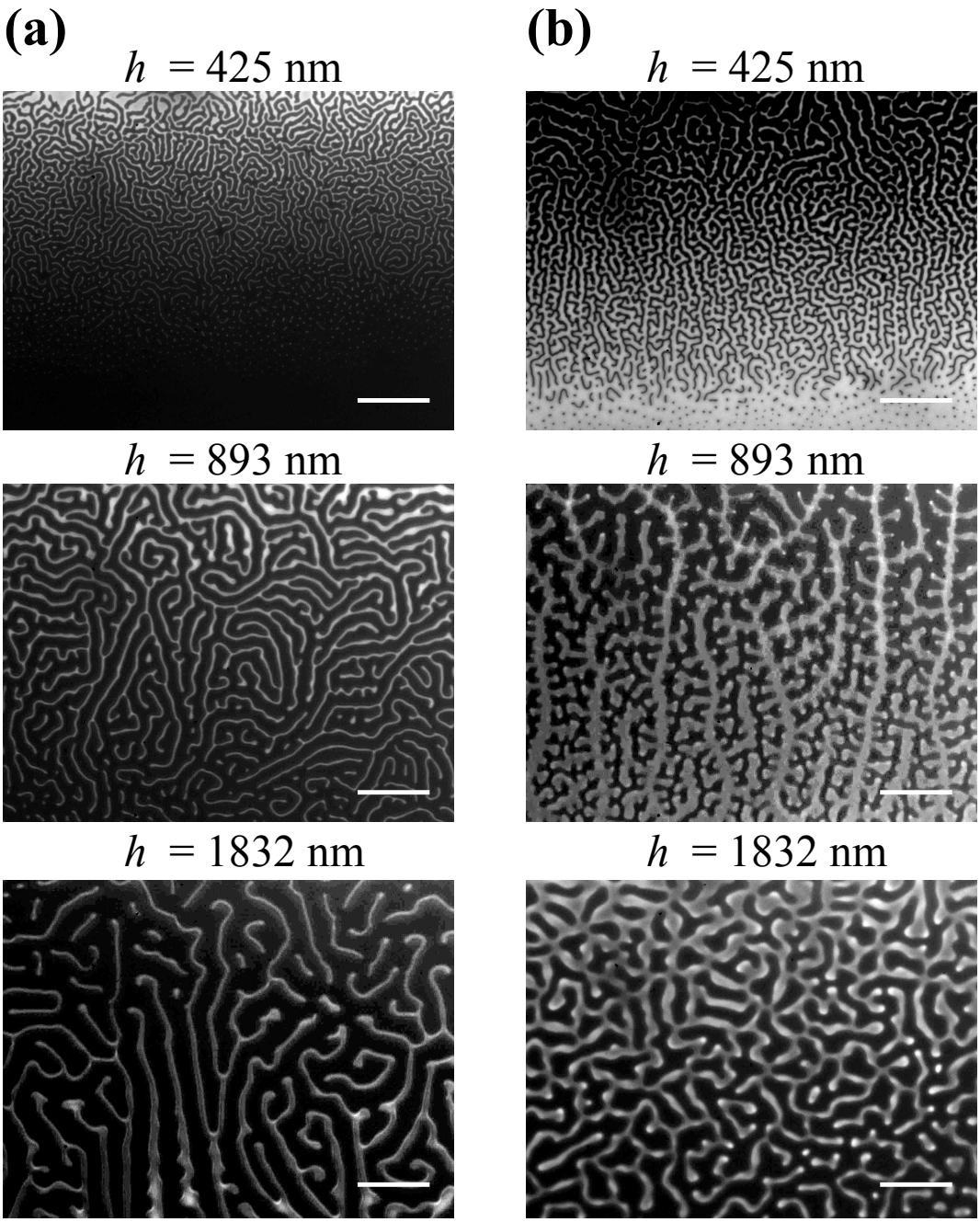

Figure 3.2: Sample images of the instability pattern formed via cylindrical indentation with a cylindrical lens. (a) – These images show the pattern morphology created by pushing the indenter into the film. (b) – These images show the pattern morphology created by pulling the indenter away from the film. All images have been contrast-edited so the patterns are easier to see. Scale bars are 20 μm.

radially outward from the centre – each bin represented the sum of the intensity of the FFT inside a given annulus, measured from the centre of the FFT. This binned intensity was then plotted as a function of inverse wavelength, and the background intensity coming from the central bright spot in the FFT was subtracted. This left a single peak defining the inverse wavelength. This final peak was fit to a parabola. The inverse wavelength that corresponded to the maximum of the fitted parabola was inverted to become the measured wavelength. Figure 3.3 shows images of some of these steps beginning with a sample raw image and ending with the measured wavelength. This analysis method is also discussed in Chapter 4 and is highlighted in fig. 3 of the Ch. 4 paper, which shows sample images and their corresponding Fourier rings and inverse wavelength peaks. Each SIS film was indented once, and five images of varying positions along the resulting instability pattern were taken. Wavelength was analyzed for each image, with the final measured wavelength for a given film thickness calculated by averaging the measured wavelength of the five images with the error being the standard deviation.

This cylindrical indentation method was unique because it allowed for two different instability morphologies to be measured simultaneously. The geometry of the cylindrical lens acting as the indenter allowed for the creation of fingering labyrinth patterns during bonding, and trident-like patterns during peeling; by rotating the indenter, both morphologies can be seen. The cylindrical indenter was large (22 cm by 20 cm) compared to the force-applying screw. When a force was applied to the cylindrical indenter to create the instability pattern, one end of the indenter was pushed into the film while the opposite end was being pulled away from the film: the force-applying screw causes the cylindrical lens to rotate on its convex face which is being pressed into the film. The 'pushing' force creates the instability pattern seen in fig. 3.2 (a) while the 'pulling' force creates a morphologically different instability pattern at the same time. Sample images of this pull-off pattern are shown in fig. 3.2 (b). These images (fig. 3.2 (b)) were analyzed using the same FFT method to create a second data set from this set of experiments.

In summary, these two sets of experiments allow two different pattern morphologies to be compared, along with two different indentation methods and two different

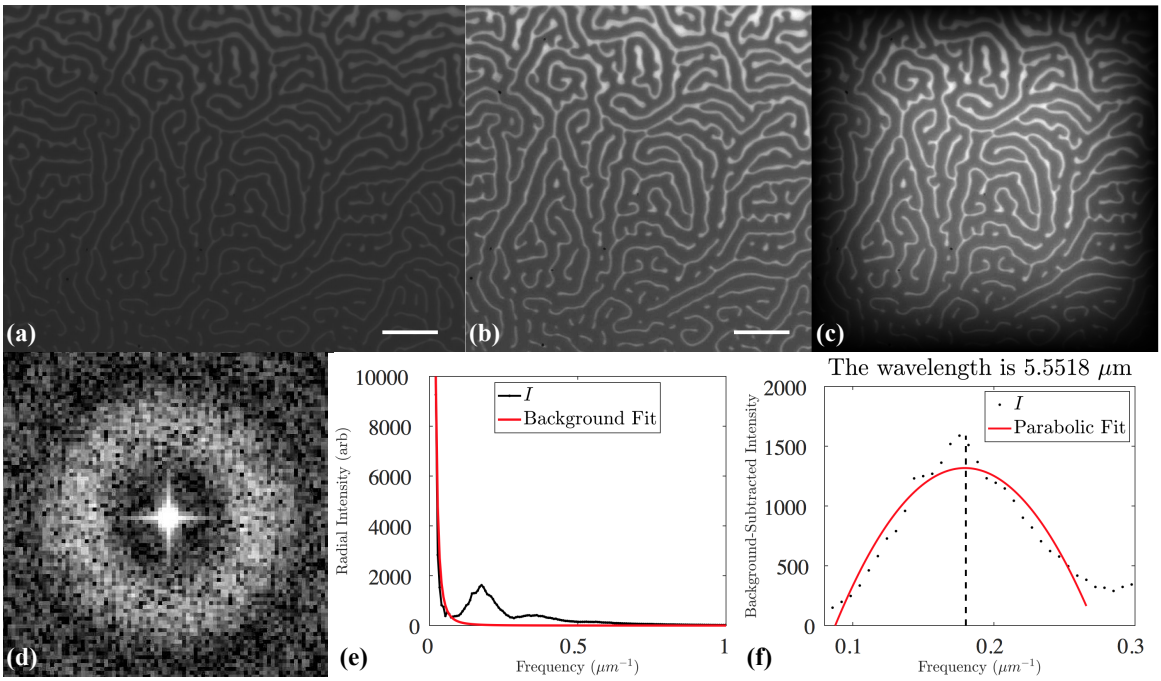

Figure 3.3: FFT analysis to extract the measured wavelength for a sample cylindrical indentation raw image. (a) – raw microscope image of the instability pattern created after indenting a 893 nm SIS film with a cylindrical indenter (second indentation method). (b) – cropped and scaled image. (c) – windowed image. (d) – FFT of the windowed image. The FFT has been contrast-enhanced for improved visibility. (e) – average radial intensity as a function of inverse wavelength. The background is fit to a function of the form a/f^b in order to isolate the first intensity peak which corresponds to the Fourier ring shown in (d). f is the frequency, while a and b are fit parameters. (f) – background-subtracted intensity as a function of inverse wavelength. The peak of interest is isolated and fit to a parabola, of which the maximum is the inverse wavelength (shown with a dotted line). The measured wavelength is stated. White scale bars in the images are 20 μm.

analysis methods. Three data sets were generated in total, comprising of 32 different SIS films and hundreds of indentations. Data from these experiments is discussed in the following section. A third set of experiments that measured wavelength using a spherical indenter were also completed. They are not discussed in this chapter because spherical indentation creates instability patterns that show the same wavelength scaling with film thickness, but the prefactor is greater than those from linear indentation experiments (like cylindrical indentation) due to the circular geometry.

This analysis is discussed in detail in Chapter 4.

3.2.2 Results and Discussion

Figure 3.4 plots wavelength as a function of film thickness for each of the three data sets discussed in the previous section. A line representing $\lambda = 4h$ is also plotted to compare to theory [12]. One can observe that all three sets of data overlap on the same plot. This confirms the expected result [24] that wavelength is independent of indentation method (when using comparable indentation geometries), and also independent of analysis method and instability morphology. The three data sets being consistent also shows that both analysis methods (direct measurement and Fourier transform) are robust. However, the data is not fully consistent with the theory curve. In fact, the data deviates from the predicted linear wavelength relationship with film thickness $\lambda \approx 4h$ particularly for films with $h < 3$ μm.

One solution to this issue might be the inclusion of an elastocapillary length term in the theory curve. To find the correct scaling relation, we can refer to the three scaling regimes outlined in the introduction of Chapter 3: eq. (3.1). We first must calculate the elastocapillary length of SIS. The shear modulus μ of SIS is approximately 0.27 MPa [35]. The surface tension γ of the SIS used is not exactly known, but it can be approximated using the known surface tensions of styrene and isoprene along with their composition ratios in SIS. Using this data [52–54], $\gamma \approx 30$ mN/m. Therefore, the elastocapillary length of SIS is $\gamma/\mu \approx 110$ nm. This number falls within the second regime given by equation (3.1b) since 110 nm is comparable to the thinnest films used in all experiments performed in this thesis. Assuming this updated scaling to be correct, we would still expect a linear wavelength relationship with film thickness but with a y-axis shift of 110/4 nm – a negligible number on this plot (fig. 3.4). Thus, the discrepancy between experiment and theory is not due to elastocapillary effects as outlined in [13].

It appears that the most commonly cited theory is not consistent with the reproducible experimental results presented here. There are many possible ways to explain this deviation. Most previous experiments measuring this instability used PDMS gels [24] whereas SIS was used for all of the experiments presented here. SIS is molecularly and structurally different from PDMS, and therefore may exhibit dif-

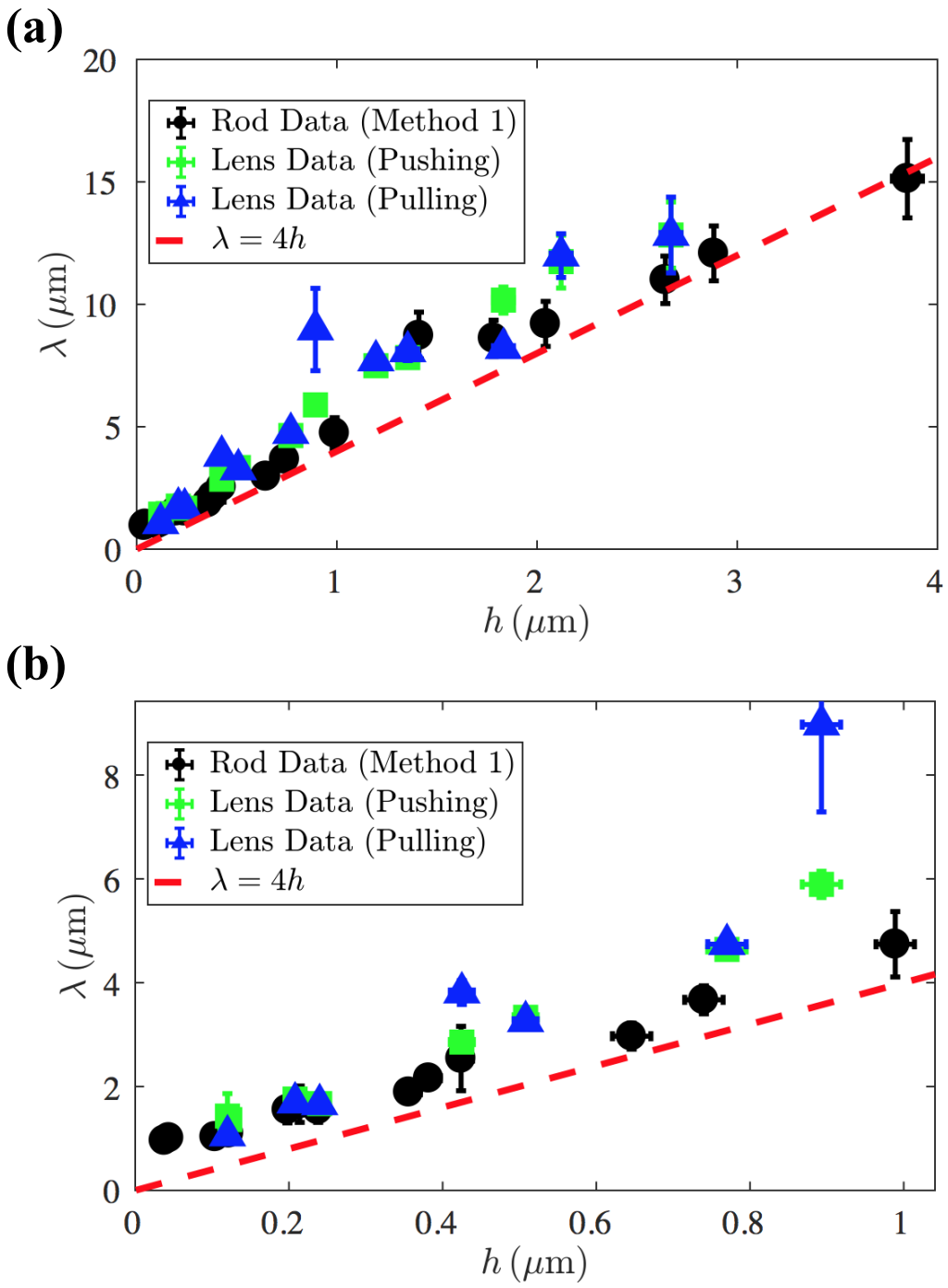

Figure 3.4: Wavelength versus film thickness. (a) displays the complete dataset, while (b) expands the data from the thinnest films for improved visibility. The plotted theory curve $\lambda = 4h$ comes from [12].

ferent material properties in thin films where molecular structure becomes important. Alternatively, the theory may not fully capture the thin film effects of this instability. This may be because substrate effects become important when working with thin films, and these substrate effects are not incorporated into the elastic adhesion-induced instability theory. We also cannot fully discount the fact that there may be some experimental parameters that were not properly controlled for that affected this deviation. Regardless, the precise physics behind the deviation between experiment and theory has not been experimentally determined. As such, the wavelength dependence on film thickness of adhesion-induced instabilities in thin SIS films remains an outstanding question.

3.3 Conclusions

In this chapter, adhesion-induced fingering instabilities were introduced. Previous studies were outlined and the literature shows that the wavelength of this instability has been found to scale linearly with film thickness. Two different indentation experiments were completed and three different data sets were obtained, measuring wavelength as a function of film thickness. Although the data was self-consistent and robust, the wavelength dependence is not fully captured by the theory. This remains an outstanding question.

In order to resolve this issue, the theory needs to be reexamined, perhaps with a focus on thin films. As well, more experiments could be performed in an attempt to find a more precise experimental wavelength dependence on film thickness in this thickness regime. Again, the focus of this thesis was studying the instability under strain, so experiments could be designed to control for more parameters to focus on the wavelength measurement instead of the instability anisotropy that will be discussed in the next chapter (Ch. 4). Some of these parameters to control for in future experiments would be applied indentation force, surface energy of the lower substrate and upper indenting surface, or thin film preparation. This may be an exciting project for a future M.Sc. student to study.

Chapter 4

Adhesion-Induced Fingering Instabilities Under Strain

This chapter outlines the most important results of the thesis which come from studying the adhesion-induced fingering instability under strain. The bulk of this chapter is the manuscript for a paper [55] that is to be submitted. I discuss the importance of this paper and the previous work that led to this study in the introduction. I also summarize the experiments and the key results from the paper before discussing further opportunities to follow up on this work in the conclusion.

4.1 Introduction

As outlined in Chapter 3, the adhesion-induced fingering instability has been well-studied experimentally, but some important issues remain unresolved and/or have not yet been examined in detail. One such study is applying a uniaxial pre-strain to a thin film prior to indentation and observing how this preparation affects instability growth upon indentation. Ghatak and Chaudhury [11] looked at how the morphology of the fingering instability is affected by a uniaxial pre-strain in films, observing that the fingers become less rounded and increasingly sawtooth-shaped with increasing strain. This study was performed using a linear indentation method.

After being made aware of this instability and beginning basic wavelength measurements, we realized that we could alter the indentation geometry by using a spher-

ical indenter to create a radial fingering instability pattern. With this indentation geometry, the resulting instability pattern upon indentation is isotropic. Applying a pre-strain to the film before indentation allows the fingers to initiate their growth from the central contact circle created by the spherical indenter, but then align along the most energetically favourable direction. This observation is easily studied using this type of geometry. In this way, we are able to compare the difference in free energy for finger growth parallel or perpendicular to the pre-strain axis (along with any angle in between). This has not yet been seen in the literature. Additionally, the study performed in [11] uses films with minimum thicknesses greater than 100 microns, while our study focuses on films with thicknesses less than 1 micron. Therefore, we are at least two orders of magnitude thinner than the previous pre-strain study in the literature. This study adds to the literature of the adhesion-induced instability in thin ($h < 1$ μm) films, which is currently not well understood.

4.2 Indenting Films Under Strain

In this paper, we indented thin SIS films with a spherical indenter to observe the ensuing fingering instability pattern. We measured the wavelength of this instability pattern. Most importantly, we pre-strained SIS films before indentation to observe the effect of uniaxial pre-strain on instability growth. We characterized this effect using an order parameter, showing that the instability pattern transitions from isotropic to anisotropic with increasing pre-strain, monotonically increasing the order parameter. We showed that this pattern anisotropy develops because it is more energetically favourable for fingers to grow along the high tension axis relative to the low tension axis, confirming the experimental results with a theoretical model.

Summary of paper

Adhesion-induced fingering instabilities in thin elastic films under strain
Benjamin Davis-Purcell, Pierre Soulard, Thomas Salez, Elie Raphaël and Kari Dalnoki-Veress, to be submitted.

This paper examines how thin elastic films form adhesion-induced fingering instabilities when a strain is applied to the film. As has been previously discussed, adhesion-induced fingering instabilities have been well studied, but until this point it was unclear how the instability develops in a pre-strained film [24]. This is the first study to rigourously examine this effect experimentally, and also to provide a model to explain the experimental data. In this paper, we first confirm that we are observing the same adhesion-induced fingering instability that has been previously studied. We then observe this instability in films under strain and show that the fingering instability pattern aligns with the high tension axis. We create a model to show that fingers align along the high tension axis because this is the most energetically favourable direction for fingers to grow.

For this paper, in collaboration with my supervisor, I designed and performed all experiments, including experiments with strained films as well as unstrained films. I developed all the experimental methods and wrote all the MATLAB code to analyze the data. Additionally, I wrote the first draft of the manuscript. The theoretical model was developed by Pierre Soulard, who worked with Thomas Salez and Elie Raphaël. All parties are involved in the editing of the manuscript. (We note that this is not the final version of the manuscript, as it is still in the editing process).

EPJ manuscript No.
(will be inserted by the editor)

Adhesion-induced fingering instabilities in thin elastic films under strain

Benjamin Davis-Purcell[1], Pierre Soulard[2], Thomas Salez[2,3], Elie Raphaël[2] and Kari Dalnoki-Veress[1,2a]

[1] Department of Physics & Astronomy, McMaster University, Hamilton, Ontario, Canada, L8S 4M1
[2] Laboratoire de Physico-Chimie Théorique, UMR CNRS 7083 Gulliver, ESPCI ParisTech, PSL Research University, Paris, France.
[3] Global Station for Soft Matter, Global Institution for Collaborative Research and Education, Hokkaido University, Sapporo, Hokkaido 060-0808, Japan.

Received: date / Revised version: date

Abstract. In this study, thin elastic films supported on a rigid substrate are brought into contact with a spherical glass indenter. Upon contact, adhesive fingers emerge at the periphery of the contact patch with a characteristic wavelength. Elastic films are also pre-strained along one axis before initiation of contact, causing the fingering pattern to become anisotropic and align with the axis along which the strain was applied. This transition from isotropic to anisotropic patterning is characterized quantitatively and a simple model is developed to understand the origin of the anisotropy. We show that it is energetically favourable for a finger to align along a high tension axis.

1 Introduction

Pattern formation in thin films has been an area of great interest in soft matter physics [1–8]. Specifically, the study of elastocapillarity, which examines the often competing interaction between interfacial capillary interactions and elasticity, has become a growing area of research [9–12]. Adherent materials favourably contact solids, and the interfacial energy which drives the adhesion can induce a deformation that is dependent on the elastic modulus [13]. In this regard, when the adhesive is a thin film an instability was discovered independently by Ghatak *et al.* [14] and Mönch *et al.* [15] which results in stunning pattern formation. These groups found that fingering and labyrinth patterns form when adhesive contact is made with thin elastic films. This adhesion-induced fingering instability has been studied in multiple works [16–25] since the discovery, with much of the work summarized in 2015 by Chaudhury *et al.* [26].

Experimentally, this instability may be observed when a thin elastic film is sandwiched between two rigid surfaces. An example of the instability occurs when a film is bonded to one of the rigid surfaces, while the other rigid surface – the indenter – is brought into contact with the free film interface. When contact is made it is seldom perfect resulting in gaps due to defects, or purposefully through the use of a spacer, or upon retraction of the indenter. This gap is crucial for the instability to develop and experiments have been performed with spacers [14, 15, 17], or by ensuring complete contact is made and then minimally retracting the indenter to debond from the film [17–23]. The resulting fingering pattern has a well-defined wavelength (λ) that is found to be independent of the gap formation method (shown schematically in fig. 1(a and b)). This wavelength can be easily understood as a competition between interfacial energy which favours adhesion and the elastic cost associated with the deformation of the elastic film. The interfacial energy dictates that the elastic adhesive film preferentially contacts the rigid surfaces. However, in order for the adhesive film to span the gap

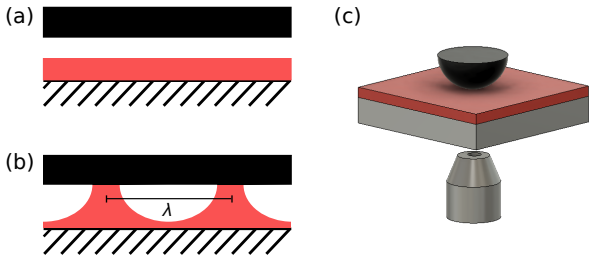

Fig. 1. (a) A spherical glass indenter (top, black) is brought close to the elastic film (red surface on substrate). (b) A characteristic wavelength (λ) forms in the elastic film when the indenter is brought into contact with the surface and contact fingers form. (c) The spherical indenter attached to a motorized actuator (not shown) is brought into contact with the elastic film and viewed from below through a clear glass slide (shown as grey lower substrate) via optical microscopy. Note that schematics are not to scale.

[a] email: dalnoki@mcmaster.ca

an elastic deformation of the film is required. The last ingredient towards understanding the instability is that the volume of the elastomeric film must be conserved (Poisson's ratio is 1/2). Thus, starting from an indenter that is some distance from the film (see fig. 1(a)) the free energy can be reduced by deforming the elastomer such that contact between the indenter and the film is made. However the deformation must be accompanied by a depletion region due to volume conservation until some distance from the finger an other finger can be formed (see schematic cross-section in fig. 1(b)). Starting from these simple assumptions, a theory can be developed which accurately captures the emergence of a natural wavelength [15,16].

In agreement with the theoretical model, numerous studies found that the wavelength depends only on the thickness of the elastic film (h), with all data from many experiments collapsing onto one master curve well fit by $\lambda = 3.8h$ [26]. Vilmin *et al.* [20] used a simple scaling argument to show that the wavelength only depends on h because of incompressibility (volume conservation), finding $\lambda \approx 4h$. A study by Gonuguntla *et al.* [18] used a linear stability analysis matched with experiments to show that for films with $h < 1$ μm, the wavelength relationship is no longer linear and depends not only on h, but also on the ratio between surface tension, γ, and shear modulus, μ. Experiments by Chakrabarti and Chaudhury [21] followed up on this work and expanded on the result, finding that $\lambda/h > 4$ for soft elastic materials where $\gamma/\mu > h$.

Multiple different aspects of this adhesion-induced fingering instability have been studied since its discovery, including finger amplitude [20] and morphology [17], as well as recent simulations and a more comprehensive theory using a cohesive-zone model [24]. However, there are still aspects of this instability which are not fully understood, as outlined in the 2015 review [26]. One such unknown is a quantitative analysis of the fingering instability in pre-strained films: Ghatak and Chaudhury showed qualitatively [19] that indenting a pre-strained film causes triangular tips of the fingers along the strain axis, but no further study was done.

In this paper, we examine the instability pattern that is created in thin elastic films when indented with a spherical indenter for films with $h < 1$ μm. We measure the wavelength of this instability and show that the scaling of wavelength with film thickness is consistent with previous work. More importantly, we present experiments where the adhesive film is uniaxially strained prior to initiating contact. We find that finger growth is more energetically favourable parallel to the strained axis. As we will show with a simple theoretical model, this is because the tension modifies the compliance of the film, making deformation easier in one direction relative to the other. Thus, the fingering instability pattern aligns along the high tension axis, creating an anisotropic pattern. Lastly, we investigate how the anisotropy in the fingering pattern increases with increasing pre-strain.

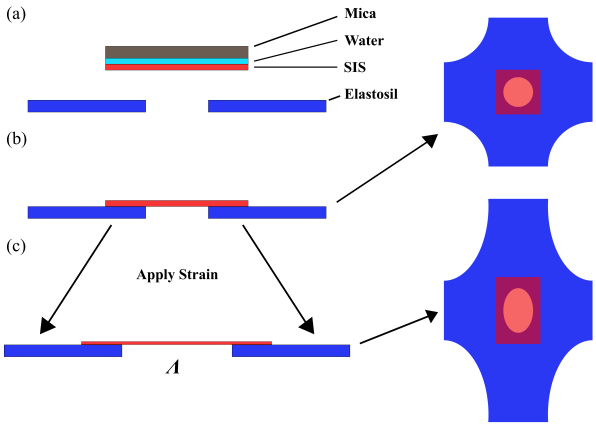

Fig. 2. Schematic of film transfer to custom-built stretching setup. (a) After the floating process, a thin layer of water remains between the mica sheet and the SIS film to allow for smooth transfer to the Elastosil (a thin elastic material) sheet. (b) The SIS film is unstrained on the Elastosil; a corresponding top view is shown. (c) A uniaxial strain is applied, causing the hole to transition from a circle to an ellipse, uniformly straining the SIS film by a factor Λ.

2 Experiment

Samples were prepared using styrene-isoprene-styrene (SIS) triblock copolymer (14% styrene content, Sigma Aldrich) which is a physically crosslinked elastomer at room temperature. SIS films were spincoated onto freshly cleaved mica sheets (Ted Pella Inc., approximately 2.5 cm×2.5 cm) from solution. These solutions were made by dissolving SIS in toluene (Fisher Scientific, Optima grade) in various concentrations to make elastomeric films of varying initial thicknesses, $h_0 = \{415, 436, 510, 705, 890\}$ nm. In addition to spincoating onto mica, one sample of each thickness was spincoated onto a silicon wafer (University Wafer) for film thickness measurement using ellipsometry (Accurion, EP3). The measured film thickness on Si is assumed to be the initial film thickness of the films spincast onto mica. About 20 films of each thickness were spincoated onto mica sheets.

The films were annealed at 108°C for 15 minutes so that the triblock was in the melt state, as well as to remove excess solvent and relax the polymer chains. The SIS films were then floated onto the surface of an ultra-pure water bath (18.2 M$\Omega \cdot$ cm). The floating films were then picked back up onto the original mica sheet such that a thin layer of water between the film and the mica was present. This floating process allows the film on mica to be transferred off of the mica sheet and onto a custom-built stretching setup, which was used to apply a strain to the film along one axis while ensuring zero strain in the perpendicular axis (see fig. 2, discussed in more detail below).

The stretching setup consisted of a sheet of Elastosil (Wacker Chemie, $h = 200\ \mu$m) cut to the shape shown schematically in fig. 2, and clamped down on each of its four edges. The shape of the Elastosil sheet was chosen such that upon stretching the sheet, a nearly uniform strain is applied to the central hole where the SIS film is deposited. Elastosil is an elastomer that has uniform thickness, is compliant and remains taught when stretched. The SIS film was transferred from the mica sheet onto the top of the Elastosil sheet, centred around the circular hole (fig. 2). Pictures of the Elastosil hole were taken before and after stretching and were analyzed by a custom Matlab program in order to obtain the strain conditions in the film. Films were stretched along the x-axis by a factor of 1 to 1.6 times their initial length, such that the extension parameter Λ varied from 1 to 1.6. Since SIS is an elastomer with Poisson's ratio $\nu \approx 1/2$, volume is conserved (i.e. no change in density upon straining). Thus, $\Lambda_x = \Lambda; \Lambda_y = 1; \Lambda_z = 1/\Lambda$. After the stretching process, films were transferred to glass microscope slides by bringing a glass microscope slide into contact with the SIS film from above. SIS preferentially sticks to glass compared to Elastosil, ensuring that the strain imposed on the SIS film remains after transfer. We emphasize that after the straining process, films that have an initial thickness of h_0 thin to a thickness of $h = h_0/\Lambda$ since $\Lambda_z = 1/\Lambda$.

In order to carry out the adhesion contact experiment the samples were placed onto an inverted optical microscope as shown schematically in fig. 1(c). The indenter, a convex spherical lens (ThorLabs Inc., with a diameter of 6 mm and focal length of 30 mm) was brought into contact with the elastic film using a precision actuator (Burleigh 8200 Inchworm) until the instability pattern formed. Images were recorded with a microscope camera (AVT GigE Vision GT1660). Sample images can be seen in fig. 3(a)-(c). Multiple experiments were carried out on each film: the indenter was retracted and re-positioned such that subsequent experiments were carried out on an undisturbed area of the film. The strains applied in this work were limited to $\Lambda \approx 1.6$, since beyond this point the thin free-standing films of SIS may begin to experience material failure. The limiting strain was less for the thinner films and any samples that showed signs of failure due to straining or defects were discarded.

3 Results and Discussion

The experimental data obtained in the experiments consist of the instability images – typical results are shown in fig. 3(a)-(c). In the images one can clearly see the central contact patch with the contact fingers radiating outwards. In the middle of the image there is no gap and there is perfect contact between the film and the indenter. The contact appears dark due to the destructive interference of light. As a result of the convex shape of the indenter the distance between the two rigid bodies increases away from the centre and eventually a gap opens up. Within this region the fingering instability is observed. The gap

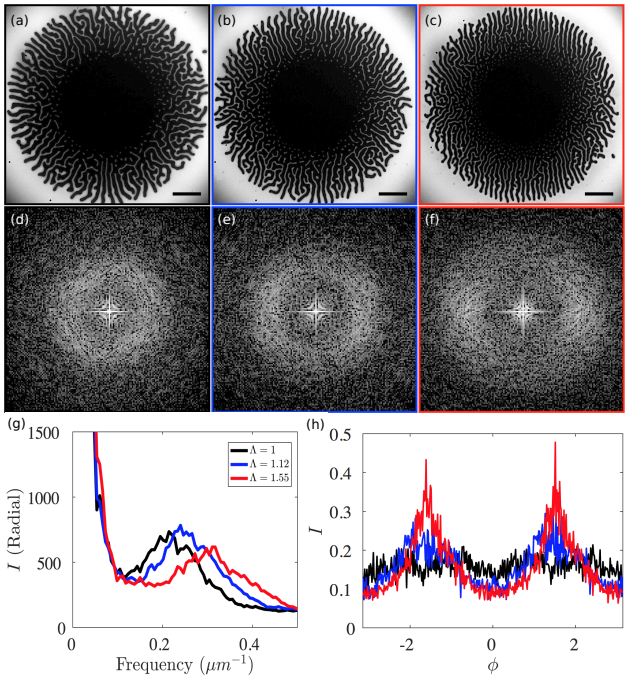

Fig. 3. Adhering fingers grow out from the centre contact patch created by the spherical indenter. For the examples shown the films have an initial thickness $h_0 = 705$ nm. The pattern becomes increasingly more anisotropic as the pre-strain in the film is increased: a) $\Lambda = 1$, b) $\Lambda = 1.12$, and c) $\Lambda = 1.55$ (scale bars are 10 μm). Corresponding FFTs ((d)-(f)) are shown below each instability image. The radial intensity average is shown in (g). The film becomes thinner as it is strained since $h = h_0/\Lambda$, which is seen here as a shifting of the peak in the radial intensity to the right with increasing strain. The angular intensity average around the Fourier ring is shown in (h) and becomes more peaked as the strain increases.

thickness increases away from the centre and the contacting fingers grow to a limiting radius where the gap is too deep – the decrease in the free energy due to adhesion is no longer sufficient to deform the elastic film and the fingers cannot grow.

We divide the following discussion of our results into four main parts. In section 3.1, we discuss the image analysis process. The wavelength and order parameter results are presented in section 3.2 and 3.3, respectively. Finally, we discuss the theory in section 3.4.

3.1 Image Analysis

To analyze this data, the two-dimensional fast Fourier transform (FFT) of each image is calculated using a custom Matlab code. Sample FFTs are shown in fig. 3(d)-(f). There are two parameters that we extract from the FFT: the wavelength λ of the instability pattern, which corresponds to the distance between consecutive fingers, and the orientation of the fingers which we characterize by an order parameter s.

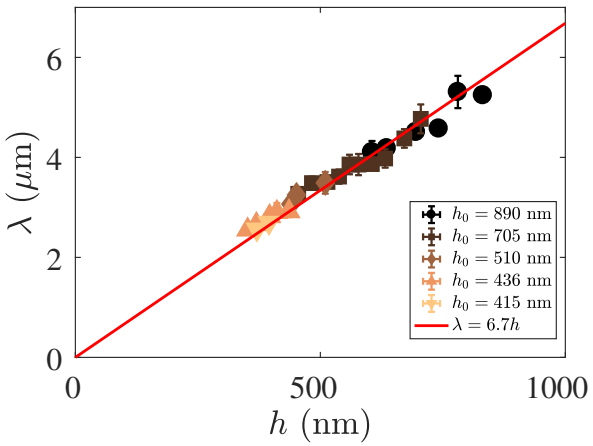

Fig. 4. Wavelength as a function of SIS film thickness. The data includes strained films, with final film thickness $h = h_0/\Lambda$. The data is fit to a line through the origin and we find the slope to be 6.7 (the larger than expected scaling is due to the spherical indentation geometry).

To calculate the wavelength, we plot the radial average of the FFT intensity as a function of inverse wavelength. This plot displays a peak corresponding to the characteristic wavelength (sample plots shown in fig. 3(g)), and the value of the maximum of this peak is the inverse wavelength, λ^{-1}. The wavelength was calculated for each image. The measured value reported for a given thickness is the average of three to eight images from multiple experiments on a single film, with the error calculated as the standard deviation. Results are discussed in section 3.2 and plotted in fig. 4.

The orientation of the pattern is encoded in the angular integral of the Fourier ring. We plot the angular average of the intensity as a function of angle, encapsulating the annulus corresponding to the Fourier ring. The annulus is defined by the radii r_+ and r_-, where $r_\pm = \left(\lambda^{-1} \pm 0.1\right)\mu\text{m}^{-1}$. Typical data can be seen in fig. 3(h). To quantify this orientation, we use an order parameter analysis similar to the order parameter that is used to calculate order in liquid crystals [27–30]. In two dimensions, the order parameter s is given by

$$s = \int \left(2\cos^2(\phi - \delta) - 1\right) \cdot I(\phi) d\phi. \qquad (1)$$

After the angular intensity $I(\phi)$ is extracted (fig. 3(h)), the intensity profiles are shifted by a small phase δ to align with the strain direction. We then calculate the order parameter using equation (1) independently for each image. Results are discussed in section 3.3.

3.2 Wavelength

Figure 4 shows the results of the wavelength analysis. The wavelength is plotted as a function of film thickness, where the final film thickness h is calculated using volume conservation as $h = h_0/\Lambda$. We find that all data falls on one master curve, with film thicknesses ranging from about 350 nm to 900 nm. The wavelength is linear as a function of film thickness, which is consistent with previous work [14,15]. The data is fit to a line forced to go through the origin as suggested by previous theoretical work and validated by experiments [16,20,26]. We find the slope of the fit to be 6.7. This is a larger value than that which has been found by most previous work, where the relation that is most agreed upon in the literature is $\lambda = 3.8h$ [26]. A recent result found a similar prefactor to that obtained in Figure 4 with $\lambda \approx 7h$ [21]. In this paper, Chakrabarti and Chaudhury suggest that this larger slope value is due to the film material having a low shear modulus (and therefore a large ratio γ/μ). The shear modulus of SIS is approximately 0.27 MPa [12] which is much higher than the modulus of the gel used in [21]. We can also approximate the ratio γ/μ of SIS given its surface tension $\gamma \approx 30$ mN/m [31–33] and find that $\gamma/\mu \approx 110$ nm; and hence $\gamma/\mu < h$ for all film thicknesses used in this study. Therefore, the mechanism for the enhanced wavelength found by Chakrabarti and Chaudhury does not appear to be the cause of the relatively large slope that we find.

We hypothesize that the large slope found in Figure 4 is a result of the spherical indentation geometry used in our experiments. Observing the typical images in fig. 3(a)-(c), one can see that the wavelength increases as the fingers move radially outwards from the centre of the contact patch. Closest to the centre, the wavelength is at its smallest value. The wavelength must increase as the radial distance increases since new fingers cannot nucleate until they are separated by a distance of at least twice the ideal value $2\lambda_0$ due to the volume depletion near a contact finger. When taking the Fourier transform, we average over all wavelengths of an image, thus we average over fingers separated by a distance of λ_0 closest to the centre of the indenter and $2\lambda_0$. The use of a spherical indentation geometry and the associated FFT averaging results in a larger wavelength than previous work with indenters that are invariant in one dimension i.e. flat or cylindrical indenters. However, the spherical indentation geometry is the optimal geometry to study the anisotropic instability growth which is the focus of this study.

3.3 Order Parameter

We calculate the order parameter s for all films as a function of relative strain in the film Λ, as outlined in section 3.1. Figure 5 shows the results of the order parameter analysis. Films that are unstrained before indentation ($\Lambda = 1$) develop isotropic fingering instability patterns upon indentation (fig. 3(a)). Perfectly disordered or isotropic radial patterns have an order parameter $s = 0$ which is consistent with the data within experimental error. Slight deviations from $s = 0$ are due to pre-stresses in the film that are incurred during the floating process.

With increasing pre-strain, the fingering pattern transitions from isotropic to anisotropic. The fingers are found

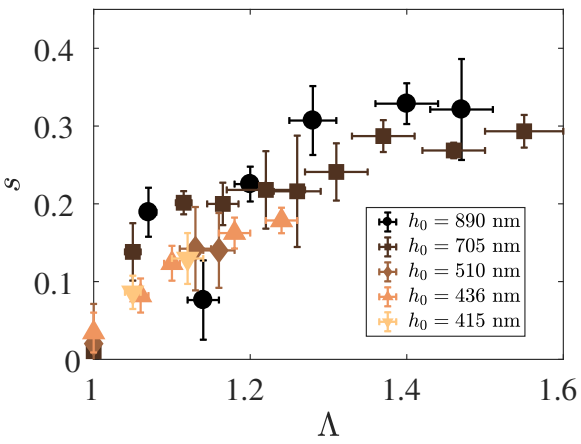

Fig. 5. Order parameter s as a function of relative extension parameter Λ. As the films are strained they become more ordered.

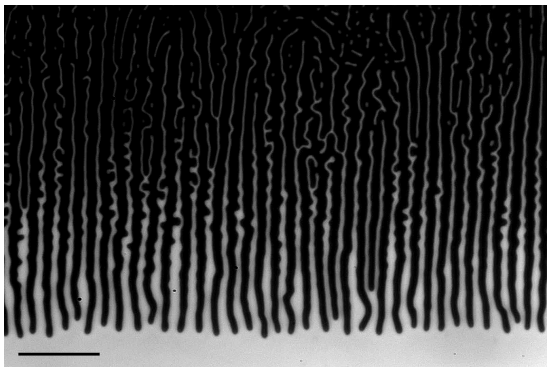

Fig. 6. A strained SIS film ($\Lambda \approx 1.5$; $h_0 \approx 900$ nm) indented with a cylindrical indenter. The resulting fingering instability pattern is almost completely anisotropic. The scale bar is 20 μm.

to align preferentially with the high tension axis, which is easily seen from the images in fig. 3(c). The order parameter is independent of film thickness since all data falls onto a single curve and s monotonically increases with the strain Λ. The theoretical maximum for s is 1, meaning perfect alignment of every finger along one axis. However, the experimental maximum is below 1. This is due to the geometry of the setup; experimentally, the fingers always bend around the circumference of the circle before aligning with the high tension axis. One can observe the fingers at the top and bottom of fig. 3(c) and observe the perfect alignment due to the strong anisotropy. In order to show that we can achieve this near-perfect anisotropy, we also present a sample image (fig. 6) of a pre-strained film ($\Lambda \approx 1.5$; $h_0 \approx 900$ nm) that has been indented with a cylindrical indenter as opposed to our spherical indenter. Here one can directly observe the complete finger growth anisotropy.

We note that SIS experiences material failure when $\Lambda \approx 1.6$ and for thinner films failure is observed at smaller values (see fig. 5). Films that fail are seen to nucleate small holes, releasing tension and are not included in the dataset.

3.4 Theory

In this section, we discuss why the fingering instability pattern aligns with the high tension axis in the film. We will not discuss the wavelength scaling theory, as this has been explored extensively in previous works [15,16,18,20, 21,26,23] and was outlined in the introduction.

When an unstrained elastomeric film is indented, an isotropic fingering instability pattern forms because there is no preferred direction of finger growth. Conversely, we observe in the experiments that when a pre-strained film is indented, an anisotropic instability pattern grows and the fingers align with the high tension axis. Qualitatively this happens because the film is more compliant perpendicular to the high tension direction. One can think of a stretched membrane: it is much easier to pinch the membrane perpendicular to the high tension, strained axis versus the parallel axis. Similarly here the elastic film which is bonded to one interface must deform in order to span the gap between the rigid surfaces. Since the film is under tension along the x-axis, it is more compliant along the perpendicular direction facilitating the deformation of the elastic surface as shown schematically in fig. 1(b). We will now show quantitatively that it is energetically favourable for a finger to grow along the high tension axis relative to the low tension axis (see fig. 2 for reference). The stress/strain analysis in this section is inspired by previous work [19,34].

We begin with a thin film in its spincoated state, O. We then stretch the film along one axis to the stretched state I. A perturbation is then applied due to indentation, which we will call state II. The matrices $\overline{\overline{F_0}}$ and $\overline{\overline{F}}$ take the film from state O to I and I to II, respectively:

$$O \xrightarrow{\overline{\overline{F_0}}} I \xrightarrow{\overline{\overline{F}}} II. \tag{2}$$

We are interested in comparing finger growth parallel to the high strain axis versus growth perpendicular to the high strain axis. Applying a strain to the film along the x-axis and assuming finger growth parallel to this axis gives the tensor

$$\overline{\overline{F_0}} = \begin{bmatrix} \Lambda & 0 & 0 \\ 0 & 1 & 0 \\ 0 & 0 & \frac{1}{\Lambda} \end{bmatrix}. \tag{3}$$

From I to II, we apply a deformation $\boldsymbol{u} = (u_1, u_2, u_3)$ to the material with $u_i = u_i(x, y, z)$. This gives

$$\overline{\overline{F}} = (1 + \boldsymbol{\nabla u})\,\overline{\overline{F_0}}. \tag{4}$$

The deformation $\boldsymbol{u}$ is applied in the x-direction (parallel to the strain direction) and along the y-direction (perpendicular to the strain direction) for comparison. $\overline{\overline{F}}$ is calculated for each deformation direction. We can then use the

strain $\overline{\overline{F}}$ to calculate the Cauchy stress tensor $\overline{\overline{\sigma}}$ to extract equations for $\boldsymbol{u}$. The Cauchy stress tensor is given by

$$\overline{\overline{\sigma}} = 2\mu\overline{\overline{FF}}^{T}, \tag{5}$$

where μ is the shear modulus and we neglect hydrostatic pressure since the elastomer is very thin. Assuming incompressibility, and using our knowledge of the equilibrium state along with boundary conditions, we solve for $\boldsymbol{u}$ and integrate to find the total elastic energy stored in one period using

$$E_{el} = \int_0^h dz \int_0^\lambda dx \; Tr\left(\boldsymbol{\nabla u} : \overline{\overline{\sigma}}\right). \tag{6}$$

Integrating separately for the parallel and perpendicular cases, we find

$$\begin{cases} E_\perp(\Lambda) = E_0(1+\Lambda^4)\text{cotanh}(\kappa h\Lambda^2) \\ E_\parallel(\Lambda) = E_0(1+\Lambda^2)\text{cotanh}(\kappa h\Lambda) \end{cases}. \tag{7}$$

with $E_0 = \frac{\pi\mu A_0^2}{4}$ where A_0 is the perturbation amplitude, and $\kappa = \frac{2\pi}{\lambda}$. We can simplify (7) by noticing that $\Lambda \approx [1, 1.6]$ and $\kappa = \frac{2\pi}{\lambda} \approx \frac{2\pi}{4h}$. Inputting these values into the hyperbolic cotangent functions, we see that $\text{cotanh}(\kappa h\Lambda^2) \approx \text{cotanh}(\kappa h\Lambda) \sim 1$. Therefore, (7) simplifies to

$$\begin{cases} E_\perp(\Lambda) = E_0(1+\Lambda^4) \\ E_\parallel(\Lambda) = E_0(1+\Lambda^2) \end{cases}. \tag{8}$$

Taking the ratio between the energy for perpendicular (to the stretch axis) finger growth and parallel finger growth, we see that

$$\frac{E_\perp}{E_\parallel} = \frac{1+\Lambda^4}{1+\Lambda^2}. \tag{9}$$

This tells us that there is a much higher energy cost for growing a finger in a direction that is perpendicular to the high tension axis versus growing a finger in a direction parallel to the high tension axis. Our result in (9) explains why fingers prefer to grow along the direction of the applied strain.

4 Conclusions

In this work, thin elastic films were indented using a spherical indentation geometry and the resulting adhesion-induced fingering instability was observed. The wavelength of the fingering pattern was measured and was found to be in agreement with the literature. Furthermore, the orientation of the fingering instability pattern was characterized quantitatively as a function of pre-strain in the film. It was found that the fingers align with the pre-strain axis. The finger order parameter was calculated as a function of pre-strain, showing that as pre-strain increases before indentation, fingers become more ordered upon indentation. The order parameter was shown to be independent of film thickness. It was shown theoretically that it is energetically favourable for the fingers created by this instability to align with the high tension axis, confirming results from experiment.

Financial Support for this work was provided by National Sciences and Engineering Research Council (NSERC). The authors would like to thank Solomon Barkley and Eric Weeks for useful discussions, and Wacker Chemie AG for donating the Elastosil material.

References

1. J. Huang, M. Juszkiewicz, W.H. de Jeu, E. Cerda, T. Emrick, N. Menon, T.P. Russell. Science **317**, 650653. (doi:10.1126/science.1144616). (2007).
2. N. Arun, A. Sharma, P. S. G. Pattader, I. Banerjee, H. M. Dixit, K. S. Narayan. Phys. Rev. Lett. **102**, 254502 (2009).
3. D. P. Holmes and A. J. Crosby. Phys. Rev. Lett. **105**, 038303 (2010).
4. P. Zhou, S. Wise, X. Li, J. Lowengrub. Phys. Rev. E **85**, 061605 (2012).
5. M. Eidini and G. H. Paulino. Sci. Adv. **1** 8, 1500224 (2015).
6. M. Leocmach, M. Nespoulous, S. Manneville, T. Gibaud. Sci. Adv. **1** 9, 1500608 (2015).
7. J. D. Paulsen, E. Hohlfeld, H. King, J. Huang, Z. Qiu, T. Russel, N. Menon, D. Vella, B. Davidovitch. PNAS **113** (5) 1144-1149, (2016).
8. M. R. Cho, J. H. Jung, M. k. Seo, S. U. Cho, Y. D. Kim, J. H. Lee, Y. S. Kim, P. Kim, J. Hone, J. Ihm, Y. D. Park. Sci. Rep. **7** 43400, (2017).
9. B. Roman and J. Bico. Journal of Physics: Condensed Matter, Volume 22, Number 49 (2010).
10. J. Weijs, B. Andreotti and J. Snoeijer. Soft Matter, **9**, 8494-8503 (2013).
11. N. D. Brubaker and J. Lega. Phil. Trans. R. Soc. A **374** 20150169 (2016).
12. R. Schulman, A. Porat, K. Charlesworth, A. Fortais, T. Salez, E. Raphaël and K. Dalnoki-Veress. Soft Matter, **13**, 720 (2017).
13. K. Kendall. Journal of Physics D: Applied Physics, Volume 4, Number 8 (1971).
14. A. Ghatak, M. Chaudhury, V. Shenoy, and A. Sharma. Phys. Rev. Lett. **85**, 4329 (2000).
15. W. Mönch and S. Herminghaus. Europhys. Lett., Volume 53, Number 4 (2001).
16. V. Shenoy and A. Sharma. Phys. Rev. Lett. **86**, 119 (2001).
17. A. Ghatak and M. Chaudhury. Langmuir 19 (7), 2621-2631 (2003). DOI: 10.1021/la026932t
18. M. Gonuguntla, A. Sharma, J. Sarkar, S. Subramanian, M. Ghosh, and V. Shenoy. Phys. Rev. Lett. **97**, 018303 (2006).
19. A. Ghatak and M. Chaudhury. The Journal of Adhesion, 83:679704, (2007).
20. T. Vilmin, F. Ziebert, E. Raphaël. Langmuir, 26 (5), pp 32573260 (2010).
21. A. Chakrabarti and M. Chaudhury. Langmuir, 29 (23), pp 69266935 (2013).
22. J. Biggins, B. Saintyves, Z. Wei, E. Bouchaud, and L. Mahadevan. PNAS 2013 110 (31) 12545-12548; doi:10.1073/pnas.1302269110 (2013).

23. B. Mukherjee, D. Dillard, R. Moore, R. Batra. International Journal of Adhesion and Adhesives, Volume 66, Pages 114-127 (2016).
24. A. Ghosh, D. Bandyopadhyay, A. Sharma. Journal of Colloid and Interface Science, Volume 477, Pages 109-122 (2016).
25. B. Mukherjee, R. Batra, D. Dillard. International Journal of Solids and Structures, Vol. 110-111, 385-403 (2017).
26. M. Chaudhury, A. Chakrabarti, and A. Ghatak. Eur. Phys. J. E **38**: 82 (2015).
27. A. Mercurieva and T. Birshtein. Makromol. Chem., Theory Simul. **1**, 205-214 (1992).
28. P. Davidson, D. Petermann, and A. M. Levelut. J. Phys. II **5**, 113 (1995).
29. F. Giesselmann, R. Germer, and A. Saipa. J. Chem. Phys. **123**, 034906 (2005).
30. A. Sanchez-Castillo, M. A. Osipov, and F. Giesselmann. Phys. Rev. E **81**, 021707 (2010).
31. B. Zuo, F. F. Zheng, Y. R. Zhao, T. Chen, Z. H. Yan, H. Ni, and X. Wang. Langmuir **28**, 4283 (2012).
32. S. Wu. J. Phys. Chem. **74**, 632 (1970).
33. L.-H. Lee. J. Polym. Sci. Pol. Phys. **5**, 1103 (1967).
34. L. Qiao and L. H. He. Eur. Phys. J. E **26**, 387-393 (2008).

4.3 Conclusions

This section presented a new study examining how an applied pre-strain in a thin elastic film affects the resulting adhesion-induced instability pattern upon indentation. Some future experiments to follow up on this study could include expanding the film thickness regime to overlap with the study in [11] by making films with thicknesses on the order of hundreds of microns. Another natural extension of this work would be to repeat the experiments using one or more different elastic materials instead of just SIS. This could include materials that are able to sustain pre-strains greater than $\Lambda \approx 1.6$ which is the maximum strain SIS can sustain. A study like this would allow one to infer the functional dependence of the order parameter on Λ, which could then be directly compared to theory.

Chapter 5

Conclusions

In this thesis, adhesion-induced fingering instabilities in thin elastic films were studied. The wavelength of the instability was investigated as a function of film thickness, expecting to corroborate previous literature work which agrees that wavelength scales linearly with film thickness. Instead, working with thin SIS films, it was observed that this scaling appears to deviate from theory for SIS films with $h < 3$ μm. It is expected that this anomaly is a thin film effect, but it remains as an outstanding question. A detailed study examining instability growth in uniaxially-strained films was also conducted. This work is reported on in a paper that is to be submitted. It was found that fingers align with the high tension axis and shown theoretically that this alignment is the minimum free energy state. When the instability pattern is induced in a pre-strained thin film, the pattern becomes increasingly anisotropic as a function of pre-strain. Maybe most importantly, the patterns created when studying this instability under strain are intricate and no pattern is exactly the same, reminding us of nature's ability to spontaneously create beauty in the most unexpected scenarios.

Bibliography

[1] Sir William Thomson F.R.S. Lx. on the equilibrium of vapour at a curved surface of liquid. *Philosophical Magazine*, 42(282):448–452, 1871.

[2] James YK Cho, Lorenzo M Polvani, et al. The morphogenesis of bands and zonal winds in the atmospheres on the giant outer planets. *SCIENCE-NEW YORK THEN WASHINGTON-*, pages 335–336, 1996.

[3] Iskra Strateva, eljko Ivezi, Gillian R. Knapp, Vijay K. Narayanan, Michael A. Strauss, James E. Gunn, Robert H. Lupton, David Schlegel, Neta A. Bahcall, Jon Brinkmann, Robert J. Brunner, Tams Budavri, Istvn Csabai, Francisco Javier Castander, Mamoru Doi, Masataka Fukugita, Zsuzsanna Gyry, Masaru Hamabe, Greg Hennessy, Takashi Ichikawa, Peter Z. Kunszt, Don Q. Lamb, Timothy A. McKay, Sadanori Okamura, Judith Racusin, Maki Sekiguchi, Donald P. Schneider, Kazuhiro Shimasaku, and Donald York. Color separation of galaxy types in the sloan digital sky survey imaging data. *The Astronomical Journal*, 122(4):1861, 2001.

[4] J Nittmann and H E Stanley. Non-deterministic approach to anisotropic growth patterns with continuously tunable morphology: the fractal properties of some real snowflakes. *Journal of Physics A: Mathematical and General*, 20(17):L1185, 1987.

[5] E. Cerda and L. Mahadevan. Geometry and physics of wrinkling. *Phys. Rev. Lett.*, 90:074302, Feb 2003.

[6] Z.Y. Huang, W. Hong, and Z. Suo. Nonlinear analyses of wrinkles in a film bonded to a compliant substrate. *Journal of the Mechanics and Physics of Solids*, 53(9):2101 – 2118, 2005.

[7] Animangsu Ghatak, Manoj K. Chaudhury, Vijay Shenoy, and Ashutosh Sharma. Meniscus instability in a thin elastic film. *Phys. Rev. Lett.*, 85:4329–4332, Nov 2000.

[8] W. Mönch and S. Herminghaus. Elastic instability of rubber films between solid bodies. *EPL (Europhysics Letters)*, 53(4):525, 2001.

[9] Animangsu Ghatak and Manoj K. Chaudhury. Adhesion-induced instability patterns in thin confined elastic film. *Langmuir*, 19(7):2621–2631, 2003.

[10] Manoj Gonuguntla, Ashutosh Sharma, Jayati Sarkar, Subash A. Subramanian, Moniraj Ghosh, and Vijay Shenoy. Contact instability in adhesion and debonding of thin elastic films. *Phys. Rev. Lett.*, 97:018303, Jul 2006.

[11] Animangsu Ghatak and Manoj K. Chaudhury. Critical confinement and elastic instability in thin solid films. *The Journal of Adhesion*, 83:679–704, 2007.

[12] Thomas Vilmin, Falko Ziebert, and Elie Raphal. Simple view on fingering instability of debonding soft elastic adhesives. *Langmuir*, 26(5):3257–3260, 2010. PMID: 19807118.

[13] Aditi Chakrabarti and Manoj K. Chaudhury. Direct measurement of the surface tension of a soft elastic hydrogel: Exploration of elastocapillary instability in adhesion. *Langmuir*, 29(23):6926–6935, 2013. PMID: 23659361.

[14] John S. Biggins, Baudouin Saintyves, Zhiyan Wei, Elisabeth Bouchaud, and L. Mahadevan. Digital instability of a confined elastic meniscus. *Proceedings of the National Academy of Sciences*, 110(31):12545–12548, 2013.

[15] Bikramjit Mukherjee, David A. Dillard, Robert B. Moore, and Romesh C. Batra. Debonding of confined elastomeric layer using cohesive zone model. *International Journal of Adhesion and Adhesives*, 66:114 – 127, 2016.

[16] M. C. Cross and P. C. Hohenberg. Pattern formation outside of equilibrium. *Rev. Mod. Phys.*, 65:851–1112, Jul 1993.

[17] A. Gierer and H. Meinhardt. A theory of biological pattern formation. *Kybernetik*, 12(1):30–39, Dec 1972.

[18] J. S. Langer. Instabilities and pattern formation in crystal growth. *Rev. Mod. Phys.*, 52:1–28, Jan 1980.

[19] William S. Wong and Alberto Salleo. *Flexible Electronics: Materials and Applications*. Springer Publishing Company, Incorporated, 1st edition, 2009.

[20] Zhihong Nie and Eugenia Kumacheva. Patterning surfaces with functional polymers. *Nature Materials*, 7:277–290, 2008.

[21] Gert Heinrich and Manfred Klppel. Rubber friction, tread deformation and tire traction. *Wear*, 265(7):1052 – 1060, 2008.

[22] B.M. Nigg, W. Herzog, and L.J. Read. Effect of viscoelastic shoe insoles on vertical impact forces in heel-toe running. *The American Journal of Sports Medicine*, 16(1):70–76, 1988. PMID: 3278635.

[23] Michael W Whittle. Generation and attenuation of transient impulsive forces beneath the foot: a review. *Gait and Posture*, 10(3):264 – 275, 1999.

[24] Manoj K. Chaudhury, Aditi Chakrabarti, and Animangsu Ghatak. Adhesion-induced instabilities and pattern formation in thin films of elastomers and gels. *Eur. Phys. J. E*, 38(7):82, 2015.

[25] P.G. de Gennes, F. Brochard-Wyart, and D. Quéré. *Capillarity and wetting phenomena*. Springer-Verlag New York, 2004.

[26] Kevin Kendall. Adhesion: Molecules and mechanics. *Science*, 263(5154):1720–1725, 1994.

[27] Nobuo Maeda, Nianhuan Chen, Matthew Tirrell, and Jacob N. Israelachvili. Adhesion and friction mechanisms of polymer-on-polymer surfaces. *Science*, 297(5580):379–382, 2002.

[28] D.A. Dillard and A.V. Pocius. *The Mechanics of Adhesion*. Elsevier Science, 2002.

[29] K. L. Johnson, K. Kendall, and A. D. Roberts. Surface energy and the contact of elastic solids. *Proceedings of the Royal Society of London A: Mathematical, Physical and Engineering Sciences*, 324(1558):301–313, 1971.

[30] L.D. Landau and E.M. Lifshitz. *Theory of Elasticity, 3rd Edition*. Pergamon Books Ltd., 1986.

[31] S. Timoshenko and J.N. Goodier. *Theory of Elasticity, 2nd Edition*. McGraw-Hill Book Company, Inc., 1951.

[32] B Roman and J Bico. Elasto-capillarity: deforming an elastic structure with a liquid droplet. *Journal of Physics: Condensed Matter*, 22(49):493101, 2010.

[33] Joost H. Weijs, Bruno Andreotti, and Jacco H. Snoeijer. Elasto-capillarity at the nanoscale: on the coupling between elasticity and surface energy in soft solids. *Soft Matter*, 9:8494–8503, 2013.

[34] N. D. Brubaker and J. Lega. Capillary-induced deformations of a thin elastic sheet. *Philosophical Transactions of the Royal Society of London A: Mathematical, Physical and Engineering Sciences*, 374(2066), 2016.

[35] Rafael D. Schulman, Amir Porat, Kathleen Charlesworth, Adam Fortais, Thomas Salez, Elie Raphael, and Kari Dalnoki-Veress. Elastocapillary bending of microfibers around liquid droplets. *Soft Matter*, 13:720–724, 2017.

[36] R. A. L. Jones. *Soft condensed matter*. Oxford University Press, USA, 2002.

[37] Hugues Bodiguel and Christian Fretigny. Reduced viscosity in thin polymer films. *Phys. Rev. Lett.*, 97:266105, Dec 2006.

[38] K. Shin, S. Obukhov, J. Chen, J. Huh, Y. Hwang, S. Mok, P. Dobriyal, P. Thiyagarajan, and T. P. Russell. Enhanced mobility of confined polymers. *Nat Mater*, 6(12):961–965, 2007.

[39] K. Thomas, A. Chenneviere, G. Reiter, and U. Steiner. Nonequilibrium behavior of thin polymer films. *Phys. Rev. E*, 83(2):021804, 2011.

[40] Joshua D. McGraw, Paul D. Fowler, Melissa L. Ferrari, and Kari Dalnoki-Veress. Relaxation of non-equilibrium entanglement networks in thin polymer films. *The European Physical Journal E*, 36(1):7, Jan 2013.

[41] Alexandre Rothen. The ellipsometer, an apparatus to measure thicknesses of thin surface films. *Review of Scientific Instruments*, 16(2):26–30, 1945.

[42] Frank L McCrackin, Elio Passaglia, Robert R Stromberg, and Harold L Steinberg. Measurement of the thickness and refractive index of very thin films and the optical properties of surfaces by ellipsometry. *J. Res. Nat. Bur. Sec. A*, 67, 1963.

[43] Abraham Ulman. *An Introduction to Ultrathin Organic Films: From Langmuir–Blodgett to Self–Assembly*. Academic press, 2013.

[44] J. Y. Chung, K. H. Kim, M. K. Chaudhury, J. Sarkar, and A. Sharma. Confinement-induced instability and adhesive failure between dissimilar thin elastic films. *The European Physical Journal E*, 20(1):47–53, May 2006.

[45] N. Arun, A. Sharma, V.B. Shenoy, and K.S. Narayan. Electric-field-controlled surface instabilities in soft elastic films. *Advanced Materials*, 18(5):660–663, 2006.

[46] Rabibrata Mukherjee, Ravindra C. Pangule, Ashutosh Sharma, and Indrani Banerjee. Contact instability of thin elastic films on patterned substrates. *The Journal of Chemical Physics*, 127(6):064703, 2007.

[47] Jayati Sarkar, Ashutosh Sharma, and Vijay Shenoy. Adhesion and debonding of soft elastic films: crack patterns, metastable pathways, and forces. *Langmuir*, 21(4):1457–1469, 2005. PMID: 15697295.

[48] Abir Ghosh, Dipankar Bandyopadhyay, and Ashutosh Sharma. Influence of the mutable kinetic parameters on the adhesion and debonding of thin viscoelastic films. *Journal of Colloid and Interface Science*, 477:109 – 122, 2016.

[49] Vijay Shenoy and Ashutosh Sharma. Pattern formation in a thin solid film with interactions. *Phys. Rev. Lett.*, 86:119–122, Jan 2001.

[50] Shi-Qing Huang, Qun-Yang Li, Xi-Qiao Feng, and Shou-Wen Yu. Pattern instability of a soft elastic thin film under van der waals forces. *Mechanics of Materials*, 38(1):88 – 99, 2006. Macro-, Meso-, Micro- and Nano-Mechanics of Materials.

[51] M Adda-Bedia and L Mahadevan. Crack-front instability in a confined elastic film. *Proceedings of the Royal Society of London A: Mathematical, Physical and Engineering Sciences*, 462(2075):3233–3251, 2006.

[52] Biao Zuo, Fan Fan Zheng, Yu Rong Zhao, TianYu Chen, Zhuo Hua Yan, Huagang Ni, and Xinping Wang. Stickslip phenomenon in measurements of dynamic contact angles and surface viscoelasticity of poly(styrene-b-isoprene-b-styrene) triblock copolymers. *Langmuir*, 28(9):4283–4292, 2012. PMID: 22329614.

[53] Souheng Wu. Surface and interfacial tensions of polymer melts. ii. poly(methyl methacrylate), poly(n-butyl methacrylate), and polystyrene. *The Journal of Physical Chemistry*, 74(3):632–638, 1970.

[54] Lieng-Huang Lee. Adhesion of high polymers. ii. wettability of elastomers. *Journal of Polymer Science Part A-2: Polymer Physics*, 5(6):1103–1118, 1967.

[55] Benjamin Davis-Purcell, Pierre Soulard, Thomas Salez, Elie Raphaël, and Kari Dalnoki-Veress. Adhesion-induced fingering instabilities in thin elastic films under strain. *(to be submitted).*